

---

# Measuring and Controlling Solution Degeneracy across Task-Trained Recurrent Neural Networks

---

Ann Huang<sup>1,2,3</sup>, Satpreet H. Singh<sup>2,3</sup>, Flavio Martinelli<sup>2,3,4</sup>, Kanaka Rajan<sup>2,3</sup>

<sup>1</sup>Harvard University   <sup>2</sup>Harvard Medical School   <sup>3</sup>Kempner Institute   <sup>4</sup>EPFL  
annhuang@g.harvard.edu

## Abstract

Task-trained recurrent neural networks (RNNs) are widely used in neuroscience and machine learning to model dynamical computations. To gain mechanistic insight into how neural systems solve tasks, prior work often reverse-engineers individual trained networks. However, different RNNs trained on the same task and achieving similar performance can exhibit strikingly different internal solutions, a phenomenon known as solution degeneracy. Here, we develop a unified framework to systematically quantify and control solution degeneracy across three levels: behavior, neural dynamics, and weight space. We apply this framework to 3,400 RNNs trained on four neuroscience-relevant tasks: flip-flop memory, sine wave generation, delayed discrimination, and path integration, while systematically varying task complexity, learning regime, network size, and regularization. We find that higher task complexity and stronger feature learning reduce degeneracy in neural dynamics but increase it in weight space, with mixed effects on behavior. In contrast, larger networks and structural regularization reduce degeneracy at all three levels. These findings empirically validate the Contravariance Principle and provide practical guidance for researchers seeking to tune the variability of RNN solutions, either to uncover shared neural mechanisms or to model the individual variability observed in biological systems. This work provides a principled framework for quantifying and controlling solution degeneracy in task-trained RNNs, offering new tools for building more interpretable and biologically grounded models of neural computation.

## 1 Introduction

Recurrent neural networks (RNNs) are widely used in machine learning and computational neuroscience to model dynamical processes. They are typically trained with standard nonconvex optimization methods and have proven useful as surrogate models for generating hypotheses about the neural mechanisms underlying task performance [1, 2, 3, 4, 5, 6]. Traditionally, the study of task-trained RNNs has focused on reverse-engineering a single trained model, implicitly assuming that networks trained on the same task would converge to similar solutions, even when initialized or trained differently. However, recent work has shown that this assumption does not hold universally, and the solution space of task-trained RNNs can be highly degenerate: networks may achieve the same level of training loss, yet differ in out-of-distribution (OOD) behavior, internal representations, neural dynamics, and connectivity [7, 8, 9, 10, 11, 12, 13]. For instance, [8] found that while trained RNNs may share certain topological features, their representational geometry can vary widely. Similarly, [7] showed that task-trained networks can develop qualitatively distinct neural dynamics and OOD generalization behaviors.

These findings raise fundamental questions about the solution space of task-trained RNNs: **What factors govern the solution degeneracy across independently trained RNNs?** When the solution space of task-trained RNNs is highly degenerate, to what extent can we trust conclusions drawn from a single model instance? While feedforward networks have been extensively studied in terms of how

weight initialization and stochastic training (e.g., mini-batch gradients) lead to divergent solutions, RNNs still lack a systematic and unified understanding of the factors that govern solution degeneracy [14, 15, 16, 17, 18, 19, 20, 21, 22, 23]. Cao and Yamins [24] proposed the *Contravariance Principle*, which posits that as the computational objective (i.e., the task) becomes more complex, the solution space should become less dispersed—since fewer models can simultaneously satisfy the stricter constraints imposed by harder tasks. While this principle is intuitive and compelling, it has thus far remained largely theoretical and has not been directly validated through empirical studies.

In this paper, we introduce a unified framework for quantifying solution degeneracy at three levels: behavior, neural dynamics, and weight space (Figure 1). Leveraging this framework, we isolate four key factors that control solution degeneracy: task complexity, learning regime, network width, and structural regularization. We apply this framework in a large-scale experiment, training 50 independently initialized RNNs on each of four neuroscience-relevant tasks. By systematically varying task complexity, learning regime, network width, and regularization, we map how each factor shapes degeneracy across behavior, dynamics, and weights. We find that as task complexity increases (whether via more input–output channels, higher memory demand, or auxiliary objectives, or as networks undergo stronger feature learning), their neural dynamics become more consistent, while their weight configurations grow more variable. In contrast, increasing network size or imposing structural regularization during training reduces variability at both the dynamics and weight levels. At the behavioral level, each of these factors reliably modulates behavioral degeneracy; however, the relationship between behavioral and dynamical degeneracy is not always consistent.

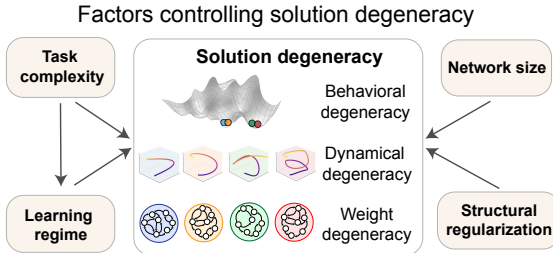


Figure 1: **Key factors shape degeneracy across behavior, dynamics, and weights.** Schematic of our framework for analyzing solution degeneracy in task-trained RNNs. We evaluate how task complexity, learning regime, network size, and structural regularization influence degeneracy at three levels: behavior (network outputs), neural dynamics (state trajectories), and weight space (connectivity).

Table 1 summarizes how task complexity, learning regime, network size, and regularization affect degeneracy across levels. In both machine learning and neuroscience, the desired level of degeneracy may vary depending on the specific research questions being investigated. This framework offers practical guidance for tailoring training to a given goal, whether encouraging consistency across models [25], or promoting diversity across learned solutions [26, 27, 28].

**Our key contributions are as follows:**

- A unified framework for analyzing solution degeneracy in task-trained RNNs across behavior, dynamics, and weights.
- A systematic sweep of four factors: task complexity, feature learning, network size, and regularization, and a summary of their effects across levels (Table 1), with practical guidance for tuning consistency vs. diversity [25, 26, 27, 28].
- A double dissociation: task complexity and feature learning yield *contravariant* effects on weights vs. dynamics, while network size and regularization yield *covariant* effects. Here, contravariant means that a factor decreases degeneracy at one level (e.g., dynamics) while increasing it at another (e.g., weights), whereas covariant means both levels change in the same direction.

**2 Methods**

**2.1 Model architecture and training procedure**

We use discrete-time nonlinear *vanilla* recurrent neural networks (RNNs), defined by the update rule:  $\mathbf{h}_t = \tanh(\mathbf{W}_h \mathbf{h}_{t-1} + \mathbf{W}_x \mathbf{x}_t + \mathbf{b})$  where  $\mathbf{h}_t \in \mathbb{R}^n$  is the hidden state,  $\mathbf{x}_t \in \mathbb{R}^m$  is the input,  $\mathbf{W}_h \in \mathbb{R}^{n \times n}$  and  $\mathbf{W}_x \in \mathbb{R}^{n \times m}$  are the recurrent and input weight matrices, and  $\mathbf{b} \in \mathbb{R}^n$  is a bias

vector. A learned linear readout is applied to the hidden state to produce the model’s output at each time step. Networks are trained with Backpropagation Through Time (BPTT) [29], which unrolls the RNN over time to compute gradients at each step. All networks are trained using supervised learning with the Adam optimizer without weight decay. Learning rates are tuned per task (Appendix B). For each task, we train 50 RNNs with 128 hidden units. Weights are initialized from the uniform distribution  $\mathcal{U}(-1/\sqrt{n}, 1/\sqrt{n})$  and hidden states are initialized to be zeros.

In all experiments, we train networks until they reach a near-asymptotic, task-specific mean-squared error (MSE) threshold on the training set (see Appendix B), after which we allow a patience period of 3 epochs and stop training to measure degeneracy. This early-stopping criterion ensures that networks trained on the same task achieve comparable final losses before any degeneracy analysis.

## 2.2 Task suite for diagnosing solution degeneracy

We selected a diverse set of four tasks designed to elicit distinct neural dynamics commonly studied in neuroscience. The **N-Bit Flip-Flop** task captures pattern recognition and memory retrieval processes, analogous to Hopfield-type attractor networks that store discrete binary patterns and retrieve them from partial cues [30, 31]. The **Delayed Discrimination** task models working memory maintenance in classic delayed-response paradigms [32, 33]. The **Sine Wave Generation** task represents pattern generation, analogous to Central Pattern Generators (CPGs) that produce self-sustaining rhythmic outputs underlying motor control [34], as well as oscillatory activity observed in motor cortex during movement [35]. Finally, the **Path Integration** task is inspired by hippocampal and entorhinal circuits that build a cognitive map of the environment to track position by integrating self-motion cues [36]. These tasks have also been used in prior benchmark suites for neuroscience-relevant RNN training [37, 38, 8], underscoring their broad relevance for studying diverse neural computations. Below, we briefly describe the task structure and the typical dynamics required to solve each one.

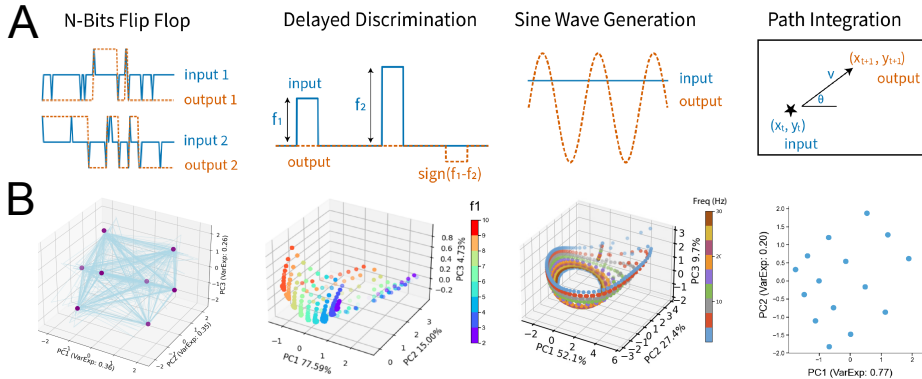


Figure 2: **Our task suite spans memory, integration, pattern generation, and decision-making.** Task schematics and representative network trajectories projected onto the top principal components are shown in (A)–(B). The four tasks are: **N-Bit Flip-Flop:** The network must remember the last nonzero input on each of  $N$  independent channels. **Delayed Discrimination:** The network compares the magnitude of two pulses, separated by a variable delay, and outputs their sign difference. **Sine Wave Generation:** A static input specifies a target frequency, and the network generates the corresponding sine wave over time. **Path Integration:** The network integrates velocity inputs to track position in a bounded 2D or 3D arena (schematic shows 2D case).

**N-Bit Flip-Flop Task** Each RNN receives  $N$  independent input channels taking values in  $\{-1, 0, +1\}$ , which switch with probability  $p_{\text{switch}}$ . The network has  $N$  output channels that must retain the most recent nonzero input on their respective channels. The network dynamics form  $2^N$  fixed points, corresponding to all binary combinations of  $\{-1, +1\}^N$ . The output range of this task is  $[-1, 1]$  and we apply an early-stopping training MSE threshold at 0.001.

**Delayed Discrimination Task** The network receives two pulses of amplitudes  $f_1, f_2 \in [2, 10]$ , separated by a variable delay  $t \in [5, 20]$  time steps, and must output  $\text{sign}(f_2 - f_1)$ . In the  $N$ -channel variant, comparisons are made independently across channels. The network forms task-relevant fixed

points to retain the amplitude of  $f_1$  during the delay period. The output range of this task is  $[-1, 1]$  and we apply an early-stopping training MSE threshold at 0.01.

**Sine Wave Generation** The network receives a static input specifying a target frequency  $f \in [1, 30]$  and must generate the corresponding sine wave  $\sin(2\pi ft)$  over time. We define  $N_{\text{freq}}$  target frequencies, evenly spaced within the range  $[1, 30]$ , and use them during training. In the  $N$ -channel variant, each input channel specifies a frequency, and the corresponding output channel generates a sine wave at that frequency. For each frequency, the network dynamics form and traverse a limit cycle that produces the corresponding sine wave. The output range of this task is  $[-1, 1]$  and we apply an early-stopping training MSE threshold at 0.05.

**Path Integration Task** Starting from a random position in 2D, the network receives angular direction  $\theta$  and speed  $v$  at each time step and updates its position estimate. In the 3D variant, the network takes as input azimuth  $\theta$ , elevation  $\phi$ , and speed  $v$ , and outputs updated  $(x, y, z)$  position. The network performs path integration by accumulating velocity vectors based on the input directions and speeds. After training, the network forms a map of the environment in its internal state space. The output range of this task is  $[-5, 5]$  and we apply an early-stopping training MSE threshold at 0.05.

In our task suite, trained RNNs develop distinct stable dynamical objects: fixed-point (N-Bit Flip Flop, Delayed Discrimination), limit cycle (Sine Wave Generation), and attractor manifold (Path Integration). In Appendix E, we extend our task suite to include a next-step prediction task on the Lorenz 96 chaotic attractors [39], where networks exhibit chaotic dynamical regime.

## 2.3 Multi-level framework for quantifying degeneracy

### 2.3.1 Behavioral degeneracy

We define a novel metric for behavioral degeneracy as the variability in network responses to out-of-distribution (OOD) inputs. We quantify OOD performance as the mean squared error of all converged networks that achieved near-asymptotic training loss under a *temporal generalization* condition. For the Delayed Discrimination task, we doubled the delay period. For all other tasks, we doubled the length of the entire trial to assess generalization under extended temporal contexts. Behavioral degeneracy is defined as standard deviation of the OOD losses:  $\sigma_{\text{OOD}} = \sqrt{\frac{1}{N} \sum_{i=1}^N (\mathcal{L}_{\text{OOD}}^{(i)} - \bar{\mathcal{L}}_{\text{OOD}})^2}$ ,

where  $\bar{\mathcal{L}}_{\text{OOD}}$  is the mean OOD loss. While we focus primarily on the *temporal generalization* condition for behavioral degeneracy since it directly probes RNNs’ sequence processing capacities and their ability to generalize across extended temporal horizons, the same metric can be readily applied to other OOD conditions, such as input noise or external perturbations. In the rest of the paper, we use the term *behavioral degeneracy [temporal generalization]* to explicitly indicate the OOD condition being tested.

### 2.3.2 Dynamical degeneracy

We use Dynamical Similarity Analysis (DSA) [40] to compare the neural dynamics of task-trained networks through pairwise analyses. While previous comparison methods mostly focus on geometry of the data [41, 42, 43, 44], RNNs implement computations through time-varying trajectories rather than static representations, and two RNNs exhibiting similar representational geometry can implement distinct dynamical computations, and vice versa. DSA compares the topological structure of the neural dynamics and has been shown to be more robust to noise and better at identifying behaviorally relevant differences than geometry-based comparison method [45]. For a pair of networks  $X$  and  $Y$ , DSA projects their time series of activities to a higher-dimensional space and identifies a linear dynamic operator for each system via next-step prediction. The DSA distance between two systems is then computed by minimizing the Frobenius norm between the operators, up to an orthogonal transformation (rotation and reflection):

$$d_{\text{DSA}}(A_x, A_y) = \min_{C \in O(n)} \|A_x - CA_y C^{-1}\|_F,$$

where  $O(n)$  is the orthogonal group. We define dynamical degeneracy as the average DSA distance across all network pairs. Additional details on the DSA metric are provided in Appendix F. We note that scale of the DSA distance used to quantify dynamical degeneracy can depend on the choice of DSA hyperparameters. To ensure fair comparison across conditions, we keep all DSA

hyperparameters fixed for RNNs trained on the same task. To assess if the neural dynamics across different trained networks are statistically different, we also establish a null distribution by comparing neural trajectories sampled from the same underlying network, see Appendix F.3 for details.

We focus on comparing neural dynamics because RNNs implement computations through time-evolving trajectories rather than static input representations. In addition, we assess representational degeneracy using Singular Vector Canonical Correlation Analysis (SVCCA) [41]. As shown in Appendix G, the four factors that influence dynamical degeneracy do not impose the same constraints on representational degeneracy.

### 2.3.3 Weight degeneracy

We quantify weight-level degeneracy via a permutation-invariant version of the Frobenius norm, defined as:

$$d_{PIF}(\mathbf{W}_1, \mathbf{W}_2) = \min_{\mathbf{P} \in \mathcal{P}(n)} \|\mathbf{W}_1 - \mathbf{P}^\top \mathbf{W}_2 \mathbf{P}\|_F$$

where  $\mathbf{W}_1$  and  $\mathbf{W}_2$  are the recurrent weight matrices for a pair of RNNs,  $\mathcal{P}(n)$  is the set of permutation matrices of size  $n \times n$ , and  $\|\cdot\|_F$  denotes the Frobenius distance. See Appendix F.2 for additional details. For comparing  $d_{PIF}$  computed on networks of different sizes, we normalize the above norm by the number of parameters in the weight matrix.

## 3 Results

### 3.1 Task complexity modulates degeneracy across levels

To investigate how task complexity influences dynamical degeneracy, we varied the number of independent input–output channels. This increased the representational load by forcing networks to solve multiple input–output mappings simultaneously. To visualize how neural dynamics vary across networks, we applied two-dimensional Multidimensional Scaling (MDS) to their pairwise distances. As task complexity increased, network dynamics became more similar, forming tighter clusters in the MDS space (Figure 3A). This contravariant relationship between task complexity and dynamical degeneracy was consistent across all tasks (Figure 3B). Higher task demands constrain the space of viable dynamical solutions, leading to greater consistency across independently trained networks.

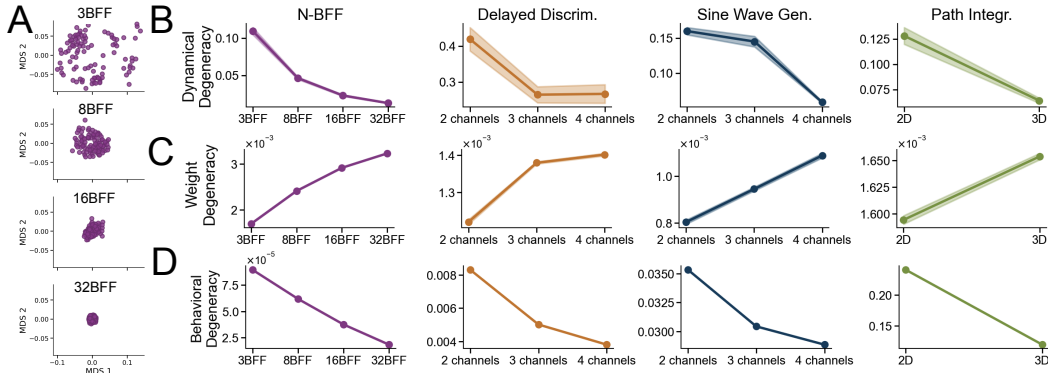


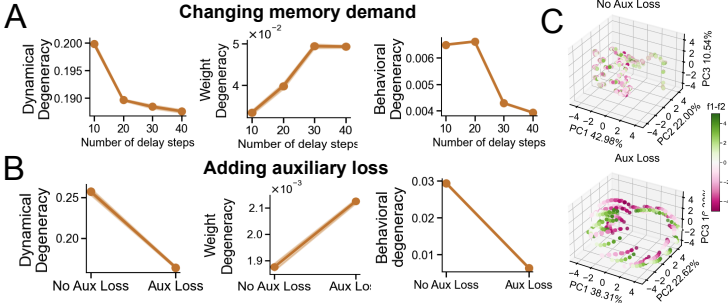
**Figure 3: Higher task complexity reduces dynamical and behavioral degeneracy, but increases weight degeneracy.** (A) Two-dimensional MDS embedding of network dynamics shows that independently trained networks converge to more similar trajectories as task complexity increases. (B) Dynamical, (C) weight, and (D) behavioral degeneracy [temporal generalization] across 50 networks as a function of task complexity. Shaded area indicates  $\pm 1$  standard error.

At the behavioral level, networks trained on more complex tasks consistently showed lower variability in their responses to OOD test inputs (Figure 3D) in the temporal generalization condition. This finding suggests that increased task complexity, by reducing dynamical degeneracy, also leads to more consistent and less degenerate behavior on the temporal generalization condition across networks. Together, the results at the behavioral and dynamical levels support the *Contravariance Principle*, which posits an inverse relationship between task complexity and the dispersion of network solutions [24].

At the weight level, we found that pairwise distances between converged RNNs’ weight matrices increased consistently with task complexity (Figure 3C). This likely reflects increased dispersion of local minima in weight space for harder tasks. This interpretation is consistent with prior work on mode averaging and loss landscape geometry in feedforward networks, showing that harder tasks tend to yield increasingly isolated minima, separated by steeper barriers [46, 47, 48, 49, 50, 51, 52]. A complementary perspective comes from [53] who introduced the *intrinsic dimension* as the lowest-dimensional weight subspace that still contains a solution, which can serve as a proxy for task complexity. As task complexity increases, the intrinsic dimension of the weight space expands and each solution occupies a thinner slice of a higher-dimensional space, leading to minima that lie further apart. In Section 3.2, we propose an additional mechanism: an interaction between task complexity and the network’s learning regime that further amplifies weight-space degeneracy.

### 3.1.1 Additional axes of task complexity

In earlier experiments, we controlled task complexity by varying the number of independent input–output channels, effectively duplicating the task across dimensions. Here, we explore two alternative approaches: increasing the task’s memory demand and adding auxiliary objectives.



**Changing memory demand.** Of the four tasks, only Delayed Discrimination requires extended memory, as its performance depends on maintaining the first stimulus across a variable delay. See Appendix D for a quantification of each task’s memory demand. We increased the memory load in Delayed Discrimination by lengthening the delay period. This manipulation reduced degeneracy at the dynamical and behavioral levels but increased it at the weight level, mirroring the effect of increasing task dimensionality (Figure 4A).

**Adding auxiliary loss.** We next examined how adding an auxiliary loss affects solution degeneracy in the Delayed Discrimination task. Specifically, the network outputs both the sign and the magnitude of the difference between two stimulus values ( $f_2 - f_1$ ), using separate output channels for each. This manipulation added a second output channel and increased memory demand by requiring the network to track the magnitude of the difference between incoming stimuli. Consistent with our hypothesis, this manipulation reduced dynamical and behavioral degeneracy [temporal generalization] while increasing weight degeneracy (Figure 4B). Crucially, the auxiliary loss induced additional line attractors in the network dynamics, further structuring internal trajectories and aligning neural responses across networks (Figure 4C). While the auxiliary loss increases both output dimensionality and temporal memory demand, we interpret its effect holistically as a structured increase in task complexity.

Figure 4: **Increasing memory demand or adding auxiliary loss changes task complexity, which in turn modulates degeneracy.** In the Delayed Discrimination task, both manipulations reduce dynamical and behavioral degeneracy [temporal generalization] while increasing weight degeneracy. The auxiliary loss also induces additional line attractors in the network’s dynamics, as shown in (C).

## 3.2 Feature learning

### 3.2.1 Task complexity scales feature learning

In deep learning theory, neural networks can either solve tasks using their random features at initialization, or adapt their weights and internal features to capture task specific structure [54, 55, 56, 57]. These are referred to as the *lazy learning* regime, where weights and internal features remain largely unchanged during training, and the *rich learning*, or *feature learning* regime, where networks reshape their hidden representations and weights to capture task-specific structure [54, 58, 59, 55]. As the complexity of a task grows, the initial random features no longer suffice to solve it, pushing the network beyond the lazy regime and into feature learning, where weights and internal representations

adapt more substantially. [60, 61]. If more complex task variants, like those in Section 3.1, truly induce greater feature learning, then networks should adapt more from their initializations and traverse a greater distance in the weight space, resulting in more dispersed final weights.

We therefore hypothesize that the increased weight degeneracy observed in harder tasks reflects stronger feature learning within the network. To test this idea, we measured feature learning strength in networks trained on different task variants using two complementary metrics [62, 58]: **Weight-change norm**:  $\|\mathbf{W}_T - \mathbf{W}_0\|_F$ , where larger values indicate stronger feature learning. **Kernel alignment (KA)**: The geometry of learning under gradient descent can be described by the neural tangent kernel (NTK), which captures how weight updates affect the network outputs. The NTK is defined by  $K = \nabla_W \hat{y}^\top \nabla_W \hat{y}$  where  $\hat{y}$  denotes the network output. KA measures the directional change of the NTK before and after training:  $\text{KA}(K^{(T)}, K^{(0)}) = \frac{\text{Tr}(K^{(T)} K^{(0)})}{\|K^{(T)}\|_F \|K^{(0)}\|_F}$ . Lower KA indicates greater NTK rotation and thus stronger feature learning.

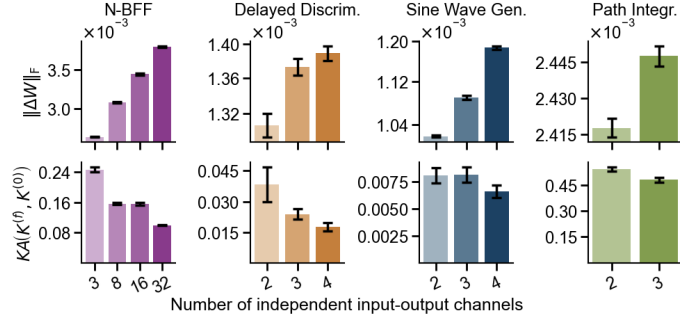


Figure 5: **More complex tasks drive stronger feature learning in RNNs.** Increased input–output dimensionality leads to higher weight-change norms ( $\|\Delta W\|_F$ ) and lower kernel alignment (KA). Error bars indicate  $\pm 1$  standard error.

We find that more complex tasks consistently drive stronger feature learning and greater dispersion in weight space, as reflected by increasing weight-change norm and decreasing kernel alignment across all tasks (Figure 5).

### 3.2.2 Controlling feature learning reshapes degeneracy across levels

Our earlier results show that harder tasks induce stronger feature learning, which in turn shapes the dispersion of solutions in the weight space. To test whether feature learning *causally* affects degeneracy, we used a principled network parameterization known as maximum update parameterization ( $\mu P$ ), which allows stable feature learning across network widths, even in the infinite-width limit [57, 54, 56, 55]. In this setup, a single hyperparameter ( $\gamma$ ) controls the strength of feature learning: higher  $\gamma$  values induce a richer feature-learning regime. Under this parameterization, the network update rule, initialization, and learning rate are scaled with respect to network width  $N$ . For the Adam optimizer, the output is scaled as  $f(t) = \frac{1}{\gamma N} W_{\text{readout}} \phi(h(t))$ . The hidden state update is scaled as  $h(t+1) - h(t) = \tau \left( -h(t) + \frac{1}{N} J \phi(h(t)) + Ux(t) \right)$ , where  $J_{ij} \sim \mathcal{N}(0, N)$  are the recurrent weights and  $\phi$  is the *tanh* nonlinearity. The learning rate scales as  $\eta = \gamma \eta_0$ . A detailed explanation of  $\mu P$  and its relationship to the standard parameterization is in Appendix K and L. For each task, we trained networks with multiple  $\gamma$  values and confirmed that larger  $\gamma$  consistently induces stronger feature learning, as evidenced by increased weight-change norm and decreased kernel alignment (Appendix M).

We observed that stronger feature learning reduced degeneracy at the dynamical level but increased it at the weight level. We see that when  $\gamma$  is high, networks tend to learn similar task-specific features and converge to consistent dynamics and behavior. In contrast, lazy networks (with small  $\gamma$ ) rely on their initial random features, leading to more divergent solutions across seeds—even though their weights move less overall (Figure 6). This finding aligns with prior work in feedforward networks, where feature learning was shown to reduce the variance of the neural tangent kernel across converged models [60]. At the behavioral level, however, increasing feature-learning strength leads networks to overfit the training distribution (Appendix J.2). We hypothesize that stronger feature learning exacerbates overfitting, increasing both average OOD loss and the variability of OOD behavior across models (Figure 6) [63, 64, 65, 66]. Although stronger feature learning increases behavioral degeneracy [temporal generalization], this may partially reflect overfitting to the training distribution,

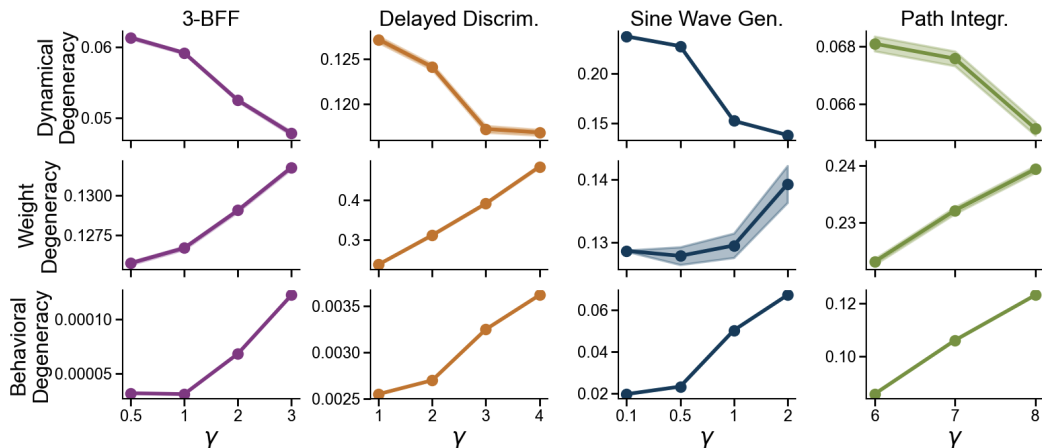


Figure 6: **Stronger feature learning reduces dynamical degeneracy but increases weight and behavioral degeneracy.** Panels show degeneracy at the dynamical, weight, and behavioral levels (top to bottom). Shaded area indicates  $\pm 1$  standard error.

an effect we highlight in Appendix J.2. Clarifying the mechanistic link between dynamical and behavioral degeneracy [temporal generalization] remains an important direction for future work. In Appendix I, we demonstrate that the observed effects of feature learning on degeneracy both interpolates smoothly within the range of  $\gamma$  values and extrapolates beyond the range reported in Figure 6.

### 3.3 Larger networks yield more consistent solutions across levels

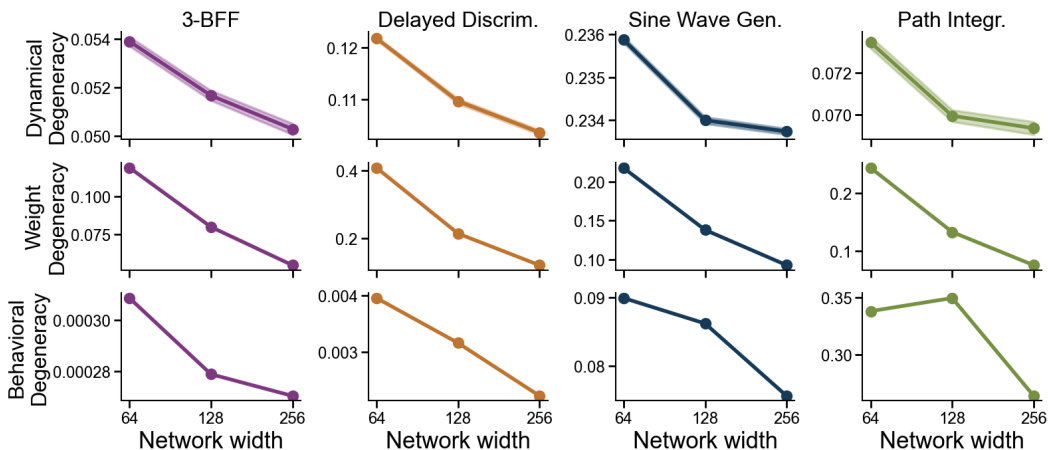


Figure 7: **Larger networks reduce degeneracy across weight, dynamics, and behavior.** After controlling for feature learning strength ( $\gamma = 1$  held constant across network widths), wider RNNs yield more consistent solutions across all three levels of analysis. Panels show degeneracy at the dynamical, weight, and behavioral levels (top to bottom). Shaded area indicates  $\pm 1$  standard error.

Prior work in machine learning and optimization shows that over-parameterization improves convergence by helping gradient methods escape saddle points [67, 68, 69, 70, 71, 72, 16]. We therefore hypothesized that larger RNNs would converge to more consistent solutions across seeds. However, increasing width also tends to push models towards the lazy regime, where feature learning is suppressed [73, 59, 54, 55, 56]. To disentangle these competing effects, we again use the  $\mu P$  parameterization, which holds feature learning strength constant (via fixed  $\gamma$ ) while scaling width. Although larger networks may yield more consistent solutions via self-averaging, this outcome is not guaranteed without controlling for feature learning. In standard RNNs, increasing width often

Table 1: Summary of how each factor affects solution degeneracy. Arrows indicate the direction of change for each level as the factor increases. Contravariant factors shift **dynamic** and **weight degeneracy** in opposite direction; covariant factors shift them in the same directions.

Factor	Dynamics	Weights	Behavior
Higher Task complexity (contravariant)	↓	↑	↓
More Feature learning (contravariant)	↓	↑	↑
Larger Network size (covariant)	↓	↓	↓
Regularization (covariant)	↓	↓	↓

induces lazier dynamics, which can paradoxically increase dynamical degeneracy rather than reduce it. The  $\mu P$  setup enables us to isolate the size effect cleanly.

Across all tasks, larger networks consistently exhibit lower degeneracy at the weight, dynamical, and behavioral levels, producing more consistent solutions across random seeds (Figure 7). Our dense sweep over 12 intermediate network sizes from 32 to 512 on the 3-Bits Flip Flop task in Appendix I further confirms the observed effect of network width on degeneracy. This pattern aligns with findings in vision and language models, where wider networks converge to more similar internal representations [74, 75, 41, 76, 77, 65]. In recurrent networks, only a few studies have investigated this “convergence-with-scale” effect using representation-based metrics [74, 78]. Our results extend these findings by (1) focusing on neural computations across time (i.e., neural dynamics) rather than static representations, and (2) demonstrating convergence-with-scale across weight, dynamical, and behavioral levels in RNNs.

### 3.4 Structural regularization reduces solution degeneracy

Low-rank and sparsity constraints are widely used structural regularizers in neuroscience-inspired modeling and efficient machine learning [4, 79, 80, 81, 82]. A low-rank penalty compresses the weight matrices into a few dominant modes, while an  $\ell_1$  penalty drives many parameters to zero and induces sparsity. In both cases, task-irrelevant features are pruned, nudging independently initialized networks toward more consistent solutions on the same task. To test this idea, we augmented the task loss with either a nuclear-norm penalty on the recurrent weights  $\mathcal{L} = \mathcal{L}_{\text{task}} + \lambda_{\text{rank}} \sum_{i=1}^r \sigma_i$ , where  $\sigma_i$  are the singular values of the recurrent matrix, or an  $\ell_1$  sparsity penalty:  $\mathcal{L} = \mathcal{L}_{\text{task}} + \lambda_{\ell_1} \sum_i |w_i|$ . We focused on the Delayed Discrimination task to control for baseline difficulty, and observe that both regularizers consistently reduced degeneracy across all levels. Similar effects hold in other tasks (Appendix O, Figure 8) and intermediate regularization strengths (Appendix I).

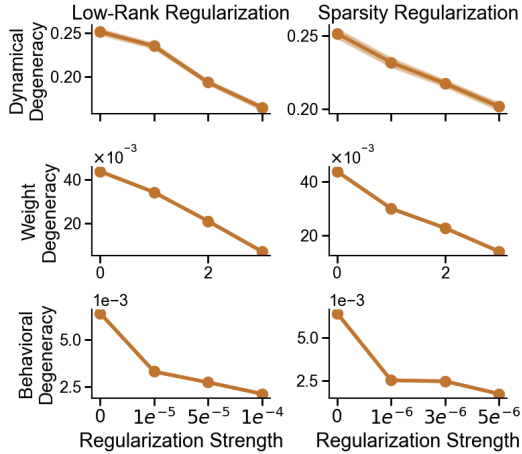


Figure 8: **Low-rank and sparsity regularization reduce solution degeneracy across all levels.** On the Delayed Discrimination task, both regularizers lower degeneracy in dynamics, weights, and behavior. Shaded area indicates  $\pm 1$  standard error.

## 4 Discussion

In this work, we introduced a unified framework for quantifying solution degeneracy in task-trained recurrent neural networks (RNNs) at three complementary levels: behavior, neural dynamics, and weights. We systematically varied four factors within our generalizable framework: (i) task complexity (via input–output dimensionality, memory demand, or auxiliary loss), (ii) feature learning strength, (iii) network size, and (iv) structural regularization. We then evaluated their effects on solution degeneracy across a diverse set of neuroscience-relevant tasks.

Two consistent patterns emerged from this analysis. First, increasing task complexity or boosting feature learning produced a **contravariant** effect: dynamical degeneracy decreased while weight degeneracy increased. Second, increasing network size or applying structural regularization reduced degeneracy at both the weight and dynamical levels—that is, a **covariant** effect. Here, covariant and contravariant refer to the relationship between weight and dynamic degeneracy, not whether degeneracy increases or decreases overall. For example, task complexity and feature learning reduce dynamical degeneracy but increase weight degeneracy, whereas network size and regularization reduce both.

We also observed that the relationship between dynamical and behavioral degeneracy depends on the varying factor. For instance, stronger feature learning leads to more consistent neural dynamics on the training task but greater variability in OOD generalization. This suggests that tightly constrained dynamics on the training set do not guarantee more consistent behavior on OOD inputs. This highlights the need for further empirical and theoretical work on how generalization depends on the internal structure of task-trained networks [83, 84, 85]. This divergence highlights a key open question: how much of behavioral consistency generalizes beyond training-aligned dynamics, and what task or network factors drive this decoupling?

These knobs allow researchers to tune the level of degeneracy in task-trained RNNs to suit specific research questions or application needs. For example, researchers may want to suppress degeneracy to study **common mechanisms** underlying a neural computation. Conversely, to probe **individual differences**, they can increase degeneracy to expose solution diversity across independently trained networks [86, 87, 88, 89]. Our framework also supports ensemble-based modeling of brain data. By comparing dynamical and behavioral degeneracy across trained networks, it may be possible to match inter-individual variability in models to that observed in animals, helping capture the full distribution of task-solving strategies [90, 91, 92, 93].

Although our analyses use artificial networks, several of the mechanisms we uncover may translate directly to experimental neuroscience. For example, introducing an auxiliary sub-task during behavioral shaping, which mirrors our auxiliary-loss manipulation, could constrain the solution space animals explore, thereby reducing behavioral degeneracy [94]. Finally, our contrasting findings motivate theoretical analysis, e.g., using linear RNNs to understand why some factors induce contravariant versus covariant relationships across behavioral, dynamical, and weight-level degeneracy.

In summary, our work takes a first step toward addressing this classic puzzle in task-driven modeling: What factors shape the variability across independently trained networks? We present a unified framework for quantifying solution degeneracy in task-trained RNNs, identify the key factors that shape the solution landscape, and provide practical guidance for controlling degeneracy to match specific research goals in neuroscience and machine learning.

**Limitations and future directions.** This work considers networks equivalent if they achieve similar training loss. Future work could extend the framework to tasks with multiple qualitatively distinct solutions, to examine whether specific factors bias the distribution of networks across those solutions. Another open question is the observed decoupling between dynamical and behavioral degeneracy: how much of behavioral consistency generalizes beyond training-aligned dynamics, and what task or network factors drive this divergence.

## 5 Acknowledgments

We acknowledge funding from NIH (RF1DA056403, U01NS136507), James S. McDonnell Foundation (220020466), Simons Foundation (Pilot Extension-00003332-02, McKnight Endowment Fund, CIFAR Azrieli Global Scholar Program, NSF (2046583), Harvard Medical School Neurobiology Lefler Small Grant Award, Harvard Medical School Dean’s Innovation Award, Alice and Joseph Brooks Fund Postdoctoral Fellowship, and Kempner Graduate Fellowship. This work has been made possible in part by a gift from the Chan Zuckerberg Initiative Foundation to establish the Kempner Institute for the Study of Natural and Artificial Intelligence at Harvard University.

## References

- [1] David Sussillo. Neural circuits as computational dynamical systems. *Current opinion in neurobiology*, 25:156–163, 2014.
- [2] Kanaka Rajan, Christopher D Harvey, and David W Tank. Recurrent network models of sequence generation and memory. *Neuron*, 90(1):128–142, 2016.
- [3] Omri Barak. Recurrent neural networks as versatile tools of neuroscience research. 46:1–6. ISSN 09594388. doi: 10.1016/j.conb.2017.06.003. URL <https://linkinghub.elsevier.com/retrieve/pii/S0959438817300429>.
- [4] Francesca Mastrogiuseppe and Srdjan Ostojic. Linking connectivity, dynamics, and computations in low-rank recurrent neural networks. *Neuron*, 99(3):609–623.e29, 2018. doi: 10.1016/j.neuron.2018.07.003.
- [5] Saurabh Vyas, Matthew D Golub, David Sussillo, and Krishna V Shenoy. Computation through neural population dynamics. *Annual Review of Neuroscience*, 43:249–275, 2020.
- [6] Laura N. Driscoll, Krishna Shenoy, and David Sussillo. Flexible multitask computation in recurrent networks utilizes shared dynamical motifs. *Nature Neuroscience*, 27(7):1349–1363, July 2024. ISSN 1097-6256, 1546-1726. doi: 10.1038/s41593-024-01668-6. URL <https://www.nature.com/articles/s41593-024-01668-6>.
- [7] Elia Turner, Kabir V Dabholkar, and Omri Barak. Charting and navigating the space of solutions for recurrent neural networks. *Advances in Neural Information Processing Systems*, 34:25320–25333, 2021.
- [8] Niru Maheswaranathan, Alex H. Williams, Matthew D. Golub, Surya Ganguli, and David Sussillo. Universality and individuality in neural dynamics across recurrent networks. In *Advances in Neural Information Processing Systems (NeurIPS)*, 2019.
- [9] Bariscan Kurtkaya, Fatih Dinc, Mert Yuksekgonul, Marta Blanco-Pozo, Ege Cirakman, Mark Schnitzer, Yucel Yemez, Hidenori Tanaka, Peng Yuan, and Nina Miolane. Dynamical phases of short-term memory mechanisms in rnns, 2025. URL <https://arxiv.org/abs/2502.17433>.
- [10] Marino Pagan, Vincent D. Tang, Mikio C. Aoi, Jonathan W. Pillow, Valerio Mante, David Sussillo, and Carlos D. Brody. Individual variability of neural computations underlying flexible decisions. *Nature*, 639(8054):421–429, March 2025. ISSN 0028-0836, 1476-4687. doi: 10.1038/s41586-024-08433-6. URL <https://www.nature.com/articles/s41586-024-08433-6>.
- [11] David G. Clark, L.F. Abbott, and Haim Sompolinsky. Symmetries and Continuous Attractors in Disordered Neural Circuits. *bioRxiv*, 2025. doi: 10.1101/2025.01.26.634933. URL <https://www.biorxiv.org/content/early/2025/01/26/2025.01.26.634933>. Publisher: Cold Spring Harbor Laboratory \_eprint: <https://www.biorxiv.org/content/early/2025/01/26/2025.01.26.634933.full.pdf>.
- [12] Janne K. Lappalainen, Fabian D. Tschopp, Sridhama Prakhya, Mason McGill, Aljoscha Nern, Kazunori Shinomiya, Shin-ya Takemura, Eyal Gruntman, Jakob H. Macke, and Srinivas C. Turaga. Connectome-constrained networks predict neural activity across the fly visual system. *Nature*, 634(8036):1132–1140, October 2024. ISSN 0028-0836, 1476-4687. doi: 10.1038/s41586-024-07939-3. URL <https://www.nature.com/articles/s41586-024-07939-3>.
- [13] Keith T. Murray. Phase codes emerge in recurrent neural networks optimized for modular arithmetic, 2025. URL <https://arxiv.org/abs/2310.07908>.
- [14] Abhramil Das and Ila R Fiete. Systematic errors in connectivity inferred from activity in strongly recurrent networks. *Nature Neuroscience*, 23(10):1286–1296, 2020.

- [15] Elia Turner and Omri Barak. The simplicity bias in multi-task rnns: shared attractors, reuse of dynamics, and geometric representation. *Advances in Neural Information Processing Systems*, 36, 2024.
- [16] Flavio Martinelli, Berfin Simsek, Wulfram Gerstner, and Johanni Brea. Expand-and-cluster: Parameter recovery of neural networks, 2024. URL <https://arxiv.org/abs/2304.12794>.
- [17] Flavio Martinelli, Alexander Van Meegen, Berfin Şimşek, Wulfram Gerstner, and Johanni Brea. Flat channels to infinity in neural loss landscapes, 2025. URL <https://arxiv.org/abs/2506.14951>.
- [18] Stanislav Fort, Huiyi Hu, and Balaji Lakshminarayanan. Deep ensembles: A loss landscape perspective. *arXiv preprint arXiv:1912.02757*, 2019.
- [19] Ian J. Goodfellow, Oriol Vinyals, and Andrew M. Saxe. Qualitatively characterizing neural network optimization problems, 2015. URL <https://arxiv.org/abs/1412.6544>.
- [20] Hao Li, Zheng Xu, Gavin Taylor, Christoph Studer, and Tom Goldstein. Visualizing the loss landscape of neural nets, 2018. URL <https://arxiv.org/abs/1712.09913>.
- [21] Stanisław Jastrzębski, Zachary Kenton, Devansh Arpit, Nicolas Ballas, Asja Fischer, Yoshua Bengio, and Amos Storkey. Three factors influencing minima in sgd, 2018. URL <https://arxiv.org/abs/1711.04623>.
- [22] Pratik Chaudhari, Anna Choromanska, Stefano Soatto, Yann LeCun, Carlo Baldassi, Christian Borgs, Jennifer Chayes, Levent Sagun, and Riccardo Zecchina. Entropy-sgd: Biasing gradient descent into wide valleys, 2017. URL <https://arxiv.org/abs/1611.01838>.
- [23] Simon Kornblith, Mohammad Norouzi, Honglak Lee, and Geoffrey Hinton. Similarity of neural network representations revisited, 2019. URL <https://arxiv.org/abs/1905.00414>.
- [24] Rosa Cao and Daniel Yamins. Explanatory models in neuroscience, part 2: Functional intelligibility and the contravariance principle. *Cognitive Systems Research*, 85:101200, 2024.
- [25] D Kepple, Rainer Engelken, and Kanaka Rajan. Curriculum learning as a tool to uncover learning principles in the brain. In *International Conference on Learning Representations*, 2022.
- [26] Samuel Liebana Garcia, Aeron Laffere, Chiara Toschi, Louisa Schilling, Jacek Podlaski, Matthias Fritsche, Peter Zátka-Haas, Yulong Li, Rafal Bogacz, Andrew Saxe, and Armin Lak. Striatal dopamine reflects individual long-term learning trajectories, December 2023. URL <http://biorxiv.org/lookup/doi/10.1101/2023.12.14.571653>.
- [27] Valeria Fascianelli, Aldo Battista, Fabio Stefanini, Satoshi Tsujimoto, Aldo Genovesio, and Stefano Fusi. Neural representational geometries reflect behavioral differences in monkeys and recurrent neural networks. *Nature Communications*, 15(1):6479, August 2024. ISSN 2041-1723. doi: 10.1038/s41467-024-50503-w. URL <https://www.nature.com/articles/s41467-024-50503-w>.
- [28] A Pan-Vazquez, Y Sanchez Araujo, B McMannon, M Louka, A Bandi, L Haetzel, International Brain Laboratory, JW Pillow, ND Daw, and IB Witten. Pre-existing visual responses in a projection-defined dopamine population explain individual learning trajectories, 2024. URL <https://europepmc.org/article/PPR/PPR811803>.
- [29] Paul J Werbos. Backpropagation through time: what it does and how to do it. *Proceedings of the IEEE*, 78(10):1550–1560, 1990.
- [30] John J. Hopfield. Neural networks and physical systems with emergent collective computational abilities. *Proceedings of the National Academy of Sciences of the United States of America*, 79(8):2554–2558, 1982.
- [31] Ignacio Jarne. Exploring flip flop memories and beyond: training recurrent neural networks with key insights. *Frontiers in Systems Neuroscience*, 2024.

- [32] Shintaro Funahashi, Charles J. Bruce, and Patricia S. Goldman-Rakic. Mnemonic coding of visual space in the monkey’s dorsolateral prefrontal cortex. *Journal of Neurophysiology*, 61(2): 331–349, 1989.
- [33] Patricia S. Goldman-Rakic. Cellular basis of working memory. *Neuron*, 14(3):477–485, 1995.
- [34] Eve Marder and Dirk Bucher. Central pattern generators and the control of rhythmic movement. *Current Biology*, 11(23):R986–R996, 2001.
- [35] Mark M. Churchland, John P. Cunningham, Matthew T. Kaufman, Justin D. Foster, Paul Nuyujukian, Stephen I. Ryu, and Krishna V. Shenoy. Neural population dynamics during reaching. *Nature*, 487(7405):51–56, 2012.
- [36] Bruce L. McNaughton, Francesco P. Battaglia, Ole Jensen, Edvard I. Moser, and May-Britt Moser. Path integration and the neural basis of the ‘cognitive map’. *Nature Reviews Neuroscience*, 7:663–678, 2006.
- [37] Guangyu R. Yang, Madhura R. Joglekar, H. Francis Song, William T. Newsome, and Xiao-Jing Wang. Task representations in neural networks trained to perform many cognitive tasks. *Nature Neuroscience*, 2019.
- [38] Mihir Khona, Shreyas Chandra, James J. Ma, and Ila R. Fiete. Winning the lottery with neural connectivity constraints: Faster learning across cognitive tasks with spatially constrained sparse rnns. *Neural Computation*, 35(11), 2023. doi: 10.1162/neco\_a\_01613.
- [39] Edward N. Lorenz. Predictability: A problem partly solved. In *ECMWF Seminar on Predictability, 4–8 September 1995*, Reading, U.K., 1996. European Centre for Medium-Range Weather Forecasts.
- [40] Mitchell Ostrow, Adam Eisen, Leo Kozachkov, and Ila Fiete. Beyond Geometry: Comparing the Temporal Structure of Computation in Neural Circuits with Dynamical Similarity Analysis, October 2023. URL <http://arxiv.org/abs/2306.10168>. arXiv:2306.10168 [cs, q-bio].
- [41] Maithra et al. Raghu. Svcca: Singular vector canonical correlation analysis for deep learning dynamics. In *NeurIPS*, 2017.
- [42] Nikolaus Kriegeskorte, Marieke Mur, and Peter Bandettini. Representational similarity analysis — connecting the branches of systems neuroscience. *Frontiers in Systems Neuroscience*, 2:4, 2008. doi: 10.3389/neuro.06.004.2008.
- [43] Alex H. Williams, Erin Kunz, Simon Kornblith, and Scott W. Linderman. Generalized Shape Metrics on Neural Representations, January 2022. URL <http://arxiv.org/abs/2110.14739>. arXiv:2110.14739 [cs, stat].
- [44] Martin Schrimpf, Jonas Kubilius, Ha Hong, Najib J. Majaj, Rishi Rajalingham, Elias B. Issa, Kohitij Kar, Pouya Bashivan, James Prescott-Roy, Kailyn Schmidt, Daniel L. K. Yamins, and James J. DiCarlo. Brain-score: Which artificial neural network for object recognition is most brain-like? *bioRxiv*, 2020. doi: 10.1101/407007. URL <https://www.biorxiv.org/content/10.1101/407007v2>.
- [45] Quentin Guilhot, Michał J Wójcik, Jascha Achterberg, and Rui Ponte Costa. Dynamical similarity analysis uniquely captures how computations develop in RNNs, 2025. URL <https://openreview.net/forum?id=pXPIQsV1St>.
- [46] Ian J. Goodfellow, Oriol Vinyals, and Andrew M. Saxe. Qualitatively characterizing neural network optimization problems. In *International Conference on Learning Representations (ICLR)*, 2015. arXiv:1412.6544.
- [47] Jonathan Frankle, Gintare Karolina Dziugaite, Daniel Roy, and Michael Carbin. Linear mode connectivity and the lottery ticket hypothesis. In *Proceedings of the 37th International Conference on Machine Learning (ICML)*, pages 3259–3269. PMLR, 2020.

- [48] James R. Lucas, Juhan Bae, Michael R. Zhang, Stanislav Fort, Richard Zemel, and Roger B. Grosse. On monotonic linear interpolation of neural network parameters. In *Proceedings of the 38th International Conference on Machine Learning (ICML)*, pages 7168–7179. PMLR, 2021.
- [49] Stanislav Fort and Stanislaw Jastrzebski. Large scale structure of neural network loss landscapes. In *Advances in Neural Information Processing Systems (NeurIPS)*, volume 32, 2019.
- [50] Alessandro Achille, Giovanni Paolini, and Stefano Soatto. Where is the information in a deep neural network? *CoRR*, abs/1905.12213, 2019.
- [51] Xingyu Qu and Samuel Horvath. Rethink model re-basin and the linear mode connectivity. *arXiv preprint arXiv:2402.05966*, 2024.
- [52] Andrew Ly and Pulin Gong. Optimization on multifractal loss landscapes explains a diverse range of geometrical and dynamical properties of deep learning. *Nature Communications*, 16(3252), 2025. doi: 10.1038/s41467-025-58532-9.
- [53] Chunyuan Li, Heerad Farkhoor, Rosanne Liu, and Jason Yosinski. Measuring the intrinsic dimension of objective landscapes. *CoRR*, abs/1804.08838, 2018.
- [54] Léon Chizat, Edouard Oyallon, and Francis Bach. On lazy training in differentiable programming. *Advances in Neural Information Processing Systems*, 32:2938–2950, 2019.
- [55] Bryan Woodworth, Suriya Gunasekar, Jason D. Lee, Nathan Srebro, Srinadh Bhojanapalli, Rina Khanna, Aaron Chatterji, and Martin Jaggi. Kernel and rich regimes in deep learning. *Journal of Machine Learning Research*, 21(243):1–48, 2020.
- [56] Mario Geiger, Stefano Spigler, Arthur Jacot, and Matthieu Wyart. Disentangling feature and lazy training in deep neural networks. *Journal of Statistical Mechanics: Theory and Experiment*, 2020(11):113301, 2020. doi: 10.1088/1742-5468/abc4de.
- [57] Blake Bordelon and Cengiz Pehlevan. Self-Consistent Dynamical Field Theory of Kernel Evolution in Wide Neural Networks, October 2022. URL <http://arxiv.org/abs/2205.09653>. arXiv:2205.09653 [stat].
- [58] Thomas George, Guillaume Lajoie, and Aristide Baratin. Lazy vs hasty: linearization in deep networks impacts learning schedule based on example difficulty. *Transactions on Machine Learning Research*, 2022, 2022. URL <https://openreview.net/forum?id=lukVf4VrfP>.
- [59] Jaehoon Lee, Yuval Bahri, Roman Novak, Samuel S. Schoenholz, Jeffrey Pennington, and Jascha Sohl-Dickstein. Wide neural networks of any depth evolve as linear models under gradient descent. In *Advances in Neural Information Processing Systems*, volume 32, pages 8572–8583, 2019.
- [60] Blake Bordelon and Cengiz Pehlevan. Dynamics of finite width Kernel and prediction fluctuations in mean field neural networks\*. *Journal of Statistical Mechanics: Theory and Experiment*, 2024(10):104021, October 2024. ISSN 1742-5468. doi: 10.1088/1742-5468/ad642b. URL <https://iopscience.iop.org/article/10.1088/1742-5468/ad642b>.
- [61] Tanishq Kumar, Blake Bordelon, Samuel J. Gershman, and Cengiz Pehlevan. Grokking as the transition from lazy to rich training dynamics. *arXiv preprint arXiv:2310.06110*, 2023. URL <https://arxiv.org/abs/2310.06110>.
- [62] Yuhan Helena Liu, Aristide Baratin, Jonathan Cornford, Stefan Mihalas, Eric Shea-Brown, and Guillaume Lajoie. How connectivity structure shapes rich and lazy learning in neural circuits. *arXiv preprint arXiv:2310.08513*, 2023. doi: 10.48550/arXiv.2310.08513. URL <https://arxiv.org/abs/2310.08513>.
- [63] Yamini Bansal, Preetum Nakkiran, and Boaz Barak. Revisiting model stitching to compare neural representations. *arXiv preprint arXiv:2106.07682*, 2021. URL <https://arxiv.org/abs/2106.07682>.

- [64] Sunny Duan, Loïc Matthey, André Saraiva, Nicholas Watters, Christopher P. Burgess, Alexander Lerchner, and Irina Higgins. Unsupervised model selection for variational disentangled representation learning. *arXiv preprint arXiv:1905.12614*, 2020. URL <https://arxiv.org/abs/1905.12614>.
- [65] Minyoung Huh, Brian Cheung, Tongzhou Wang, and Phillip Isola. The platonic representation hypothesis. *arXiv preprint arXiv:2405.07987*, 2024. URL <https://arxiv.org/abs/2405.07987>.
- [66] Yixuan Li, Jason Yosinski, Jeff Clune, Hod Lipson, and John Hopcroft. Convergent learning: Do different neural networks learn the same representations? *arXiv preprint arXiv:1511.07543*, 2016. URL <https://arxiv.org/abs/1511.07543>.
- [67] Kenji Kawaguchi. Deep learning without poor local minima. In *Advances in Neural Information Processing Systems 29*, pages 586–594, 2016.
- [68] Quynh Nguyen and Matthias Hein. The loss surface of deep and wide neural networks. *CoRR*, abs/1704.08045, 2017.
- [69] Simon S. Du, Jason D. Lee, Haochuan Li, Liwei Wang, and Xiyu Zhai. Gradient descent finds global minima of deep neural networks. *CoRR*, abs/1811.03804, 2018.
- [70] Zeyuan Allen-Zhu, Yuanzhi Li, and Zhao Song. A convergence theory for deep learning via over-parameterization. In *Proceedings of the 36th International Conference on Machine Learning*, pages 242–252, 2019.
- [71] Difan Zou, Yuan Cao, Dongruo Zhou, and Quanquan Gu. Stochastic gradient descent optimizes over-parameterized deep relu networks. *CoRR*, abs/1811.08888, 2018.
- [72] Berfin Şimşek, François Ged, Arthur Jacot, Francesco Spadaro, Clément Hongler, Wulfram Gerstner, and Johanni Brea. Geometry of the loss landscape in overparameterized neural networks: Symmetries and invariances, 2021. URL <https://arxiv.org/abs/2105.12221>.
- [73] Arthur Jacot, Franck Gabriel, and Clément Hongler. Neural tangent kernel: Convergence and generalization in neural networks. In *Advances in Neural Information Processing Systems*, volume 31, 2018.
- [74] Ari S. Morcos, Maithra Raghu, and Samy Bengio. Insights on representational similarity in neural networks with canonical correlation. In *NeurIPS*, 2018.
- [75] Simon Kornblith, Mohammad Norouzi, Honglak Lee, and Geoffrey Hinton. Similarity of neural network representations revisited. In *ICML*, 2019.
- [76] Fred Wolf, Rainer Engelken, Maximilian Puelma-Touzel, Juan Daniel Flórez Weidinger, and Andreas Neef. Dynamical models of cortical circuits. 25:228–236. ISSN 09594388. doi: 10.1016/j.conb.2014.01.017. URL <https://linkinghub.elsevier.com/retrieve/pii/S0959438814000324>.
- [77] Felix et al. Klabunde. Contrasim – analyzing neural representations based on contrastive learning. In *ICLR*, 2024.
- [78] Thao Nguyen, Maithra Raghu, and Simon Kornblith. Do wide and deep networks learn the same things? uncovering how neural network representations vary with width and depth. In *International Conference on Learning Representations (ICLR)*, 2021. URL <https://openreview.net/forum?id=KJNcAkY8tY4>. Poster.
- [79] Manuel Beiran, Alexis Dubreuil, Adrian Valente, Francesca Mastrogiuseppe, and Srdjan Ostojic. Shaping dynamics with multiple populations in low-rank recurrent networks. *arXiv preprint arXiv:2007.02062*, 2020. doi: 10.48550/arXiv.2007.02062.
- [80] Bruno A. Olshausen and David J. Field. Emergence of simple-cell receptive field properties by learning a sparse code for natural images. *Nature*, 381(6583):607–609, 1996. doi: 10.1038/381607a0.

- [81] Song Han, Jeff Pool, John Tran, and William J. Dally. Learning both weights and connections for efficient neural networks. In *Advances in Neural Information Processing Systems*, pages 1135–1143, 2015. doi: 10.48550/arXiv.1506.02626.
- [82] Xavier Glorot, Antoine Bordes, and Yoshua Bengio. Deep sparse rectifier neural networks. In *Proceedings of the 14th International Conference on Artificial Intelligence and Statistics*, volume 15, pages 315–323, 2011.
- [83] Qianyi Li, Ben Sorscher, and Haim Sompolinsky. Representations and generalization in artificial and brain neural networks. *Proceedings of the National Academy of Sciences*, 121(27):e2311805121, 2024. doi: 10.1073/pnas.2311805121.
- [84] Uri Cohen, SueYeon Chung, Daniel D. Lee, and Haim Sompolinsky. Separability and geometry of object manifolds in deep neural networks. *Nature Communications*, 11:746, 2020. doi: 10.1038/s41467-020-14578-5.
- [85] Ben Sorscher, Surya Ganguli, and Haim Sompolinsky. Neural representational geometry underlies few-shot concept learning. *Proceedings of the National Academy of Sciences*, 119(43):e2200800119, 2022. doi: 10.1073/pnas.2200800119.
- [86] Xavier Bouthillier, Pierre Delaunay, Mirko Bronzi, Assya Trofimov, Brennan Nichyporuk, Justin Szeto, Nazanin Mohammadi Sepahvand, Edward Raff, Kanika Madan, Vikram Voleti, et al. Accounting for variance in machine learning benchmarks. *Proceedings of Machine Learning and Systems*, 3:747–769, 2021.
- [87] Katharina Morik. Sloppy modeling. *Knowledge representation and organization in machine learning*, pages 107–134, 2005.
- [88] Rubing Yang, Jialin Mao, and Pratik Chaudhari. Does the data induce capacity control in deep learning? In *International Conference on Machine Learning*, pages 25166–25197. PMLR, 2022.
- [89] Satpreet H Singh, Floris van Breugel, Rajesh PN Rao, and Bingni W Brunton. Emergent behaviour and neural dynamics in artificial agents tracking odour plumes. *Nature Machine Intelligence*, 5(1):58–70, 2023.
- [90] Ignacio Negrón-Oyarzo, Nelson Espinosa, Marcelo Aguilar-Rivera, Marco Fuenzalida, Francisco Aboitiz, and Pablo Fuentealba. Coordinated prefrontal–hippocampal activity and navigation strategy-related prefrontal firing during spatial memory formation. *Proceedings of the National Academy of Sciences*, 115(27):7123–7128, 2018. doi: 10.1073/pnas.1720117115.
- [91] Zoe C. Ashwood, Nicholas A. Roy, Iris R. Stone, International Brain Laboratory, Anne E. Urai, Anne K. Churchland, Alexandre Pouget, and Jonathan W. Pillow. Mice alternate between discrete strategies during perceptual decision-making. *Nature Neuroscience*, 25:201–212, 2022. doi: 10.1038/s41593-021-01007-z.
- [92] Fanny Cazettes, Luca Mazzucato, Masayoshi Murakami, João P. Morais, Elisabete Augusto, Alfonso Renart, and Zachary F. Mainen. A reservoir of foraging decision variables in the mouse brain. *Nature Neuroscience*, 26:840–849, 2023. doi: 10.1038/s41593-023-01305-8.
- [93] Marino Pagan, Vincent D. Tang, Mikio C. Aoi, Jonathan W. Pillow, Valerio Mante, David Sussillo, and Carlos D. Brody. Individual variability of neural computations underlying flexible decisions. *Nature*, 639:421–429, 2025. doi: 10.1038/s41586-024-08433-6.
- [94] BR Howard. Control of variability. *ILAR journal*, 43(4):194–201, 2002.
- [95] Peter J Schmid. Dynamic mode decomposition and its variants. *Annual Review of Fluid Mechanics*, 54(1):225–254, 2022.
- [96] Peter H. Schönemann. A generalized solution of the orthogonal procrustes problem. *Psychometrika*, 31(1):1–10, Mar 1966. doi: 10.1007/BF02289451.

- [97] Chris Ding, Tao Li, and Michael I. Jordan. Nonnegative matrix factorization for combinatorial optimization: Spectral clustering, graph matching, and clique finding. In *Proceedings of the Eighth IEEE International Conference on Data Mining (ICDM '08)*, pages 183–192. IEEE, 2008. doi: 10.1109/ICDM.2008.130.
- [98] Fanwang Meng, Michael G. Richer, Alireza Tehrani, Jonathan La, Taewon David Kim, P. W. Ayers, and Farnaz Heidar-Zadeh. Procrustes: A python library to find transformations that maximize the similarity between matrices. *Computer Physics Communications*, 276: 108334, 2022. doi: 10.1016/j.cpc.2022.108334. URL <https://www.sciencedirect.com/science/article/pii/S0010465522000522>.
- [99] Ryan N Gutenkunst, Joshua J Waterfall, Fergal P Casey, Kevin S Brown, Christopher R Myers, and James P Sethna. Universally sloppy parameter sensitivities in systems biology models. *PLoS computational biology*, 3(10):e189, 2007.
- [100] Greg Yang, Edward J. Hu, Igor Babuschkin, Szymon Sidor, Xiaodong Liu, David Farhi, Nick Ryder, Jakub Pachocki, Weizhu Chen, and Jianfeng Gao. Tensor programs v: Tuning large neural networks via zero-shot hyperparameter transfer. *arXiv preprint arXiv:2203.03466*, 2022. doi: 10.48550/arXiv.2203.03466. Accepted at NeurIPS 2021.
- [101] Greg Yang, Dingli Yu, Chen Zhu, and Soufiane Hayou. Tensor programs vi: Feature learning in infinite-depth neural networks. *arXiv preprint arXiv:2310.02244*, 2023. doi: 10.48550/arXiv.2310.02244. Accepted at ICLR 2024.
- [102] Kenneth D Miller and Francesco Fumarola. Mathematical equivalence of two common forms of firing rate models of neural networks. *Neural computation*, 24(1):25–31, 2012.

# Appendix

## A Task details

### A.1 N-Bit Flip Flop

Task Parameter	Value
Probability of flip	0.3
Number of time steps	100

### A.2 Delayed Discrimination

Task Parameter	Value
Number of time steps	60
Max delay	20
Lowest stimulus value	2
Highest stimulus value	10

### A.3 Sine Wave Generation

Task Parameter	Value
Number of time steps	100
Time step size	0.01
Lowest frequency	1
Highest frequency	30
Number of frequencies	100

### A.4 Path Integration

Task Parameter	Value
Number of time steps	100
Maximum speed ( $v_{\max}$ )	0.4
Direction increment std ( $\theta_{\text{std}} / \phi_{\text{std}}$ )	$\pi/10$
Speed increment std	0.1
Noise std	0.0001
Mean stop duration	30
Mean go duration	50
Environment size (per side)	10

## B Training details

### B.1 N-Bit Flip Flop

Training Hyperparameter	Value
Optimizer	Adam
Learning rate	0.001
Learning rate scheduler	None
Max epochs	300
Steps per epoch	128
Batch size	256
Early stopping threshold	0.001
Patience	3
Time constant ( $\mu P$ )	1

### B.2 Delayed Discrimination

Training Hyperparameter	Value
Optimizer	Adam
Learning rate	0.001
Learning rate scheduler	CosineAnnealingWarmRestarts
Max epochs	500
Steps per epoch	128
Batch size	256
Early stopping threshold	0.01
Patience	3
Time constant ( $\mu P$ )	0.1

### B.3 Sine Wave Generation

Training Hyperparameter	Value
Optimizer	Adam
Learning rate	0.0005
Learning rate scheduler	None
Max epochs	500
Steps per epoch	128
Batch size	32
Early stopping threshold	0.05
Patience	3
Time constant ( $\mu P$ )	1

## B.4 Path Integration

Training Hyperparameter	Value
Optimizer	Adam
Learning rate	0.001
Learning rate scheduler	ReduceLROnPlateau
Learning rate decay factor	0.5
Learning rate decay patience	40
Max epochs	1000
Steps per epoch	128
Batch size	64
Early stopping threshold	0.05
Patience	3
Time constant ( $\mu P$ )	0.1

## C Task performance of trained networks

In all experiments, we train networks until they reach a **near-asymptotic, task-specific mean-squared error (MSE) threshold** (0.001 for N-BFF, 0.01 for Delayed Discrimination, and 0.05 for Sine-Wave Generation and Path Integration), after which we allow a patience period of 3 epochs and stop training to measure degeneracy. This early-stopping criterion ensures that networks trained on the same task/condition achieve comparable final losses before any degeneracy analysis.

To quantify the residual variation, we report the coefficient of variation (CV) of the final training loss across seeds for each condition, expressed as % of the mean. Header labels match the x-axis levels used in the main-text figures. Final losses cluster tightly near small values of the loss threshold, so even a double-digit CV translates to very small absolute variation. For example, a 10% CV at an MSE of 0.001 implies an s.d. of  $10^{-4}$ ; at 0.01 it's  $10^{-3}$ . Additionally, the networks converged well on a global scale. Across our experiments, the mean MSE after training is under 2% of the mean MSE at initialization, indicating that training has converged well. Individual values: 0.059% (N-BFF), 1.6% (Delayed Discrimination), 0.32% (Sine-Wave Generation), 0.94% (Path Integration). CV can look large when the mean is tiny (the denominator is small). For example, a 16% CV on Sine-Wave Generation task corresponds to 0.05% of the initialization loss, which is consistent with minor differences due to the stochastic gradients rather than under-training.

These variability values are also not monotonic in any factor and sometimes move opposite to the degeneracy trends, arguing against a loss-dispersion confound to solution degeneracy.

Table 2: Coefficient of variation (CV) of the final training loss across 50 networks for each task complexity level.

Task Complexity	Level 1	Level 2	Level 3	Level 4
N-BFF	6.30%	4.60%	9.30%	3.50%
Delayed Discrim.	15.90%	8.40%	9.50%	—
Sine Wave Gen.	9.94%	9.20%	8.70%	—
Path Integr.	9.16%	2.85%	—	—

Table 3: Coefficient of variation (CV) of the final training loss across 50 networks for each feature learning strength ( $\gamma$ )

Feature Learning Strength	$\gamma_1$	$\gamma_2$	$\gamma_3$	$\gamma_4$
N-BFF	9.70%	9.10%	13.40%	11.70%
Delayed Discrim.	8.70%	12.60%	11.70%	12.30%
Sine Wave Gen.	3.50%	3.90%	10.90%	11.70%
Path Integr.	5.40%	5.20%	6.20%	—

Table 4: Coefficient of variation (CV) of the final training loss across 50 networks for each network width.

Network Width	64 units	128 units	256 units
N-BFF	3.80%	4.20%	3.50%
Delayed Discrim.	3.30%	3.00%	3.20%
Sine Wave Gen.	17.80%	16.60%	16.40%
Path Integr.	5.10%	5.40%	5.90%

Table 5: Coefficient of variation (CV) of the final training loss across 50 networks for each L1 regularization strength.

L1 Regularization	$\lambda_1$	$\lambda_2$	$\lambda_3$	$\lambda_4$
N-BFF	2.10%	6.90%	1.10%	—
Delayed Discrim.	15.90%	14.50%	16.70%	14.90%
Sine Wave Gen.	10.40%	11.10%	11.10%	—
Path Integr.	9.00%	7.10%	3.00%	—

Table 6: Coefficient of variation (CV) of the final training loss across 50 networks for each rank regularization strength.

Rank Regularization	$\lambda_1$	$\lambda_2$	$\lambda_3$	$\lambda_4$
N-BFF	2.10%	7.20%	4.30%	—
Delayed Discrim.	15.90%	16.90%	13.60%	12.10%
Sine Wave Gen.	13.90%	14.30%	15.90%	—
Path Integr.	7.70%	7.90%	6.70%	—

## D Memory demand of each task

In this section, we quantify each task’s memory demand by measuring how far back in time its inputs influence the next output. Specifically, for each candidate history length  $h$ , we build feature vectors

$$\mathbf{s}_t^{(h)} = [x_{t-h+1}, \dots, x_t; y_t] \in \mathbb{R}^{h d_{in} + d_{out}},$$

and **train a two-layer MLP to predict the subsequent target**  $y_{t+1}$ . We then evaluate the held-out mean-squared error  $\text{MSE}(h)$ , averaged over multiple random initializations. We identify the smallest history length  $h^*$  at which the error curve plateaus or has a minimum, and take  $h^*$  as the task’s intrinsic memory demand.

From the results, we can see that the N-Bits Flip-Flop task requires only one time-step of memory—exactly what’s needed to recall the most recent nonzero input in each channel. The Sine Wave Generation task demands two time-steps, reflecting the need to track both phase and direction of change. Path Integration likewise only needs one time-step, since the current position plus instantaneous velocity and heading suffice to predict the next position. Delayed Discrimination is the only memory-intensive task: our method estimates a memory demand of 25 time-steps, which happens to be the time interval between the offset of the first stimulus and the onset of the response period, during which the network needs to first keep track of the amplitude of the first stimulus and then its decision.

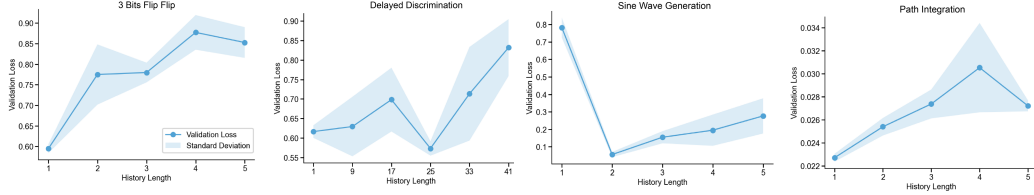


Figure 9: **Memory demand of each task.** The held-out mean-squared error  $MSE(h)$  of a two-layer MLP predictor is plotted against history length  $h$ . The intrinsic memory demand  $h^*$ , defined by the plateau or minimum of each curve, is 1 for the N-Bits Flip-Flop and Path Integration tasks, 2 for Sine Wave Generation, and 25 for Delayed Discrimination—matching the inter-stimulus delay interval in that task.

## E Solution degeneracy in chaotic RNNs

Our original task suite comprises neuroscience-motivated tasks that produce stable-attractors: fixed-point (N-Bit Flip Flop, Delayed Discrimination), limit cycle (Sine Wave Generation), and attractor manifold (Path Integration). To further demonstrate that the observed effect of the four factors on degeneracy extend to RNNs with chaotic activity, here we add a chaotic attractor task and verified that the effects of all four factors on dynamical and weight degeneracy are consistent with Table 1.

**Lorenz 96 Attractor Dataset** We simulated trajectories from the Lorenz 96 dynamical system [39], defined by

$$\frac{dx_i}{dt} = (x_{i+1} - x_{i-2})x_{i-1} - x_i + F, \quad i = 1, \dots, N,$$

with cyclic boundary conditions  $x_{-1} = x_{N-1}$ ,  $x_0 = x_N$ ,  $x_{N+1} = x_1$ . The external forcing parameter was set to  $F = 8.0$ , a standard choice that induces chaotic dynamics.

To generate the dataset, we numerically integrated the system for  $N = 16, 24$ , and 32 dimensions. Each simulation used a time step of  $\Delta t = 0.01$  and produced 15000 time points after discarding an initial transient of 1000 steps to remove non-stationary behavior. Initial conditions were sampled as small random perturbations around the fixed point  $x_i = F$ :

$$x_i(0) = F + 0.1 \varepsilon_i, \quad \varepsilon_i \sim \mathcal{N}(0, 1).$$

For each condition, we trained 50 RNNs on next-step prediction until the networks achieve a near-asymptotic MSE loss at 0.0005. After training, the average Lyapunov exponent of RNNs trained on the Lorenz 96 attractor with 16 dimensions is  $12.58 \pm 0.74$ , indicating chaotic neural dynamics.

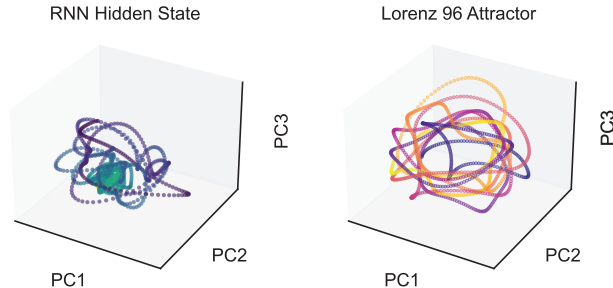


Figure 10: RNN recurrent activities and Lorenz 96 attractor ( $N = 16$ ) trajectories projected onto their respective top 3 principle components.

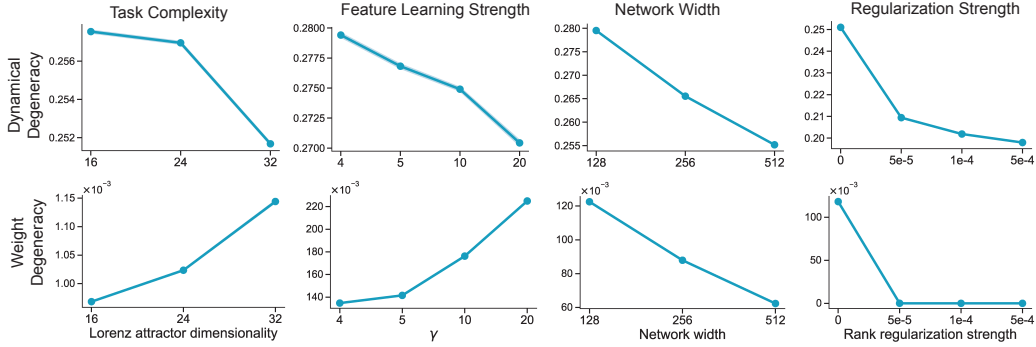


Figure 11: Varying the four factors on Lorenz 96 next-step prediction task changes solution degeneracy across the dynamical and weight level in a way that is consistent with Table 1.

## F Additional details on the degeneracy metrics

### F.1 Dynamical Degeneracy

Briefly, DSA proceeds as follows: Given two RNNs with hidden states  $\mathbf{h}_1(t) \in \mathbb{R}^n$  and  $\mathbf{h}_2(t) \in \mathbb{R}^n$ , we first generate a delay-embedded matrix,  $\mathbf{H}_1$  and  $\mathbf{H}_2$  of the hidden states in their original state space. Next, for each delay-embedded matrix, we use Dynamic Mode Decomposition (DMD) [95] to extract linear forward operators  $\mathbf{A}_1$  and  $\mathbf{A}_2$  of the two systems’ dynamics. Finally, a Procrustes distance between the two matrices  $\mathbf{A}_1$  and  $\mathbf{A}_2$  is used to quantify the dissimilarity between the two dynamical systems and provide an overall DSA score, defined as:

$$d_{\text{Procrustes}}(\mathbf{A}_1, \mathbf{A}_2) = \min_{\mathbf{Q} \in O(n)} \|\mathbf{A}_1 - \mathbf{Q}\mathbf{A}_2\mathbf{Q}^{-1}\|_F$$

where  $\mathbf{Q}$  is a rotation matrix from the orthogonal group  $O(n)$  and  $\|\cdot\|_F$  is the Frobenius norm. This metric quantifies how dissimilar the dynamics of the two RNNs are after accounting for orthogonal transformations. We quantify Dynamical Degeneracy across many RNNs as the average pairwise distance between pairs of RNN neural-dynamics (hidden-state trajectories).

After training, we extract each network’s hidden-state activations for every trial in the training set, yielding a tensor of shape (trials  $\times$  time steps  $\times$  neurons). We collapse the first two dimensions and yield a matrix of size (trials  $\times$  time steps)  $\times$  neurons. We then apply PCA to retain the components that explain 99% of the variance to remove noisy and low-variance dimensions of the hidden state trajectories. Next, we perform a grid search over candidate delay lags, with a minimum lag of 1 and a maximum lag of 30, selecting the lag that minimizes the reconstruction error of DSA on the dimensionality reduced trajectories. Finally, we fit DSA with full rank and the optimal lag to these PCA-projected trajectories and compute the pairwise DSA distances between all networks.

### F.2 Weight degeneracy

We computed the pairwise distance between the recurrent matrices from different networks using Two-sided Permutation with One Transformation [96, 97] function from the Procrustes Python package [98].

### F.3 Establishing a null distribution for dynamical and weight degeneracy

The DSA scores that we used to define the dynamical degeneracy are inherently context-dependent. Specifically, the absolute scale of DSA distances can vary with hyperparameters, particularly the delay embedding dimension and the rank used in DSA, because the underlying Procrustes analysis between two dynamics matrices relies on the Frobenius norm, which in turn depends on the dimension of the dynamic operator being compared. Following the procedure described in the original DSA paper, we fixed these hyperparameters across all groups within each task to ensure fair comparison.

To further validate the interpretation of DSA values, we computed null distributions of the DSA scores, i.e. the distribution of DSA scores when sampled neural activities come from *identical* networks. For

each of the 50 networks analyzed in Figure 3B, we randomly split the sampled neural trajectories from the same network into two subsets and computed DSA distances between them. This procedure yields a distribution of DSA scores expected from *identical dynamical systems*, which serves as a reference noise floor. The 95% confidence intervals (CIs) for these null distributions are reported below (header labels such as "Level 1" correspond to the task-complexity levels shown in the main-text figures). These CIs are, on average, an order of magnitude smaller than the computed dynamical degeneracy, indicating that the observed differences between networks trained from different initializations are statistically significant.

Table 7: Establishing a null distribution for dynamical degeneracy: 95% confidence intervals of null DSA scores computed by comparing trajectories from the same network. CIs are on average an order of magnitude smaller than across-network distances.

Task Complexity	Level 1	Level 2	Level 3	Level 4
N-BFF	[0.011, 0.013]	[0.009, 0.016]	[0.008, 0.013]	[0.006, 0.009]
Delayed Discrimination	[0.039, 0.064]	[0.014, 0.076]	[0.025, 0.032]	—
Sine Wave Generation	[0.057, 0.102]	[0.054, 0.081]	[0.048, 0.073]	—
Path Integration	[0.023, 0.037]	[0.010, 0.018]	—	—

For the PIF distance we used to define weight degeneracy, we similarly established a noise floor by *randomly permuting* each trained network’s recurrent weight matrix and computing the distance between the permuted and original matrices. The PIF metric reliably recovers a PIF distance of 0 under this null setting, confirming its robustness to noise and the meaningfulness of the reported cross-network PIF differences.

## G Representational degeneracy

We further quantified solution degeneracy at the representational level—that is, the variability in each network’s internal feature space when presented with the same input dataset—using Singular Vector Canonical Correlation Analysis (SVCCA). SVCCA works by first applying singular value decomposition (SVD) to each network’s activation matrix, isolating the principal components that capture most of its variance, and then performing canonical correlation analysis (CCA) to find the maximally correlated directions between the two reduced subspaces. The resulting canonical correlations therefore measure how similarly two networks represent the same inputs: high average correlations imply low representational degeneracy (i.e., shared feature subspaces), whereas lower correlations reveal greater divergence in what the models learn. We define the representational degeneracy (labeled as the SVCCA distance below) as

$$d_{\text{repr}}(A_x, A_y) = 1 - \text{SVCCA}(A_x, A_y).$$

We found that as we vary the four factors that robustly control the dynamical degeneracy across task-trained RNNs, the representational-level degeneracy isn’t necessarily constrained by those same factors in the same way. In RNNs, task-relevant computations are implemented at the level of network’s dynamics instead of static representations, and RNNs that implement similar temporal dynamics can have disparate representational geometry. Therefore, it is expected that task complexity, learning regime, and network size change the task-relevant computations learned by the networks by affecting their neural dynamics instead of representations. DSA captures the dynamical aspect of the neural computation by fitting a forward operator matrix  $A$  that maps the network’s activity at one time step to the next, therefore directly capturing the temporal evolution of neural activities. By contrast, SVCCA aligns the principal subspaces of activation vectors at each time point but treats those vectors as independent samples—it never examines how one state evolves into the next. As a result, SVCCA measures only static representational similarity and cannot account for the temporal dependencies that underlie RNN computations. Nonetheless, we expect SVCCA might be more helpful in measuring the solution degeneracy in feedforward networks.

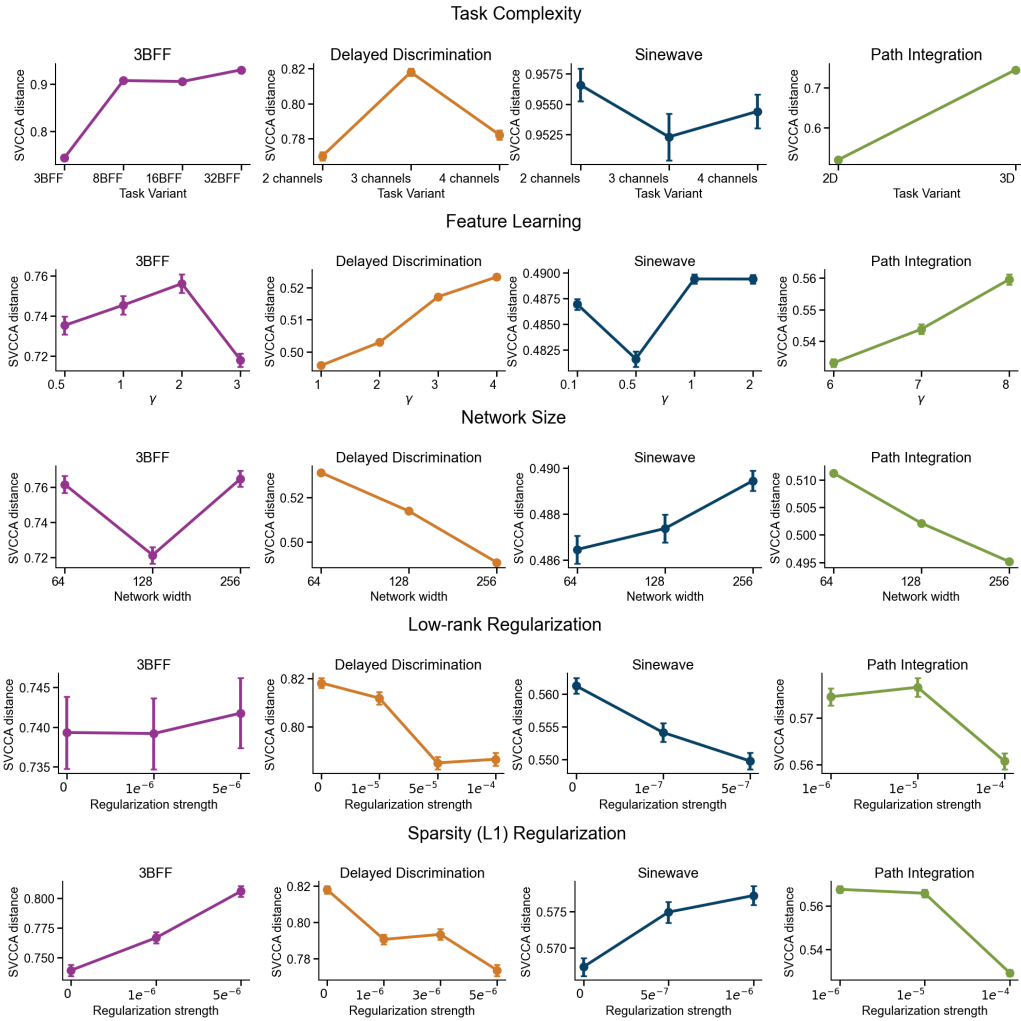


Figure 12: Representational degeneracy, as measured by the average SVCCA distance between networks, does not necessarily change uniformly as we vary task complexity, feature learning strength, network size, and regularization strength.

## H Task complexity effect on degeneracy in Gated RNNs

To examine whether the observed trends in dynamical and weight degeneracy generalize beyond vanilla RNNs, we conducted additional experiments using gated recurrent units (GRUs). Note that prior work suggests that architectural choices influence the *geometry* but not the *topology* of neural dynamics, which is primarily shaped by task structure [99]. Meanwhile, the Dynamical Similarity Analysis (DSA) metric we employ to quantify dynamical degeneracy is designed to precisely capture the topological organization of neural dynamics while remaining invariant to geometric transformations [40].

As a preliminary test, we trained GRUs on the Sine Wave Generation task while systematically varying task complexity by changing the number of input–output channels. Consistent with our findings in vanilla RNNs, increasing task complexity led to a **decrease in dynamical degeneracy** and a **rise in weight degeneracy**.

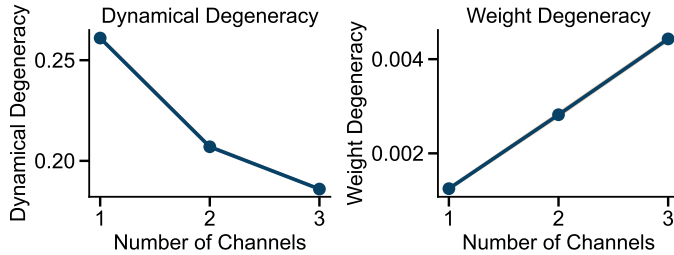


Figure 13: Increasing task complexity in the Sine Wave Generation task produces the same effect on dynamical and weight degeneracy in both vanilla RNNs and GRUs.

## I Dense sweep on feature learning, network width, and regularization strength

it is important to know whether the degeneracy trends generalize to intermediate values and beyond the ranges reported in the main paper. To test this, we used 3-BFF as an example and ran a dense sweep both interpolating within and extrapolating beyond the ranges shown in Figs. 3 and 6–8. We demonstrate that cross dynamical and weight levels, the degeneracy trends remain consistent and interpolate smoothly across these intermediate values.

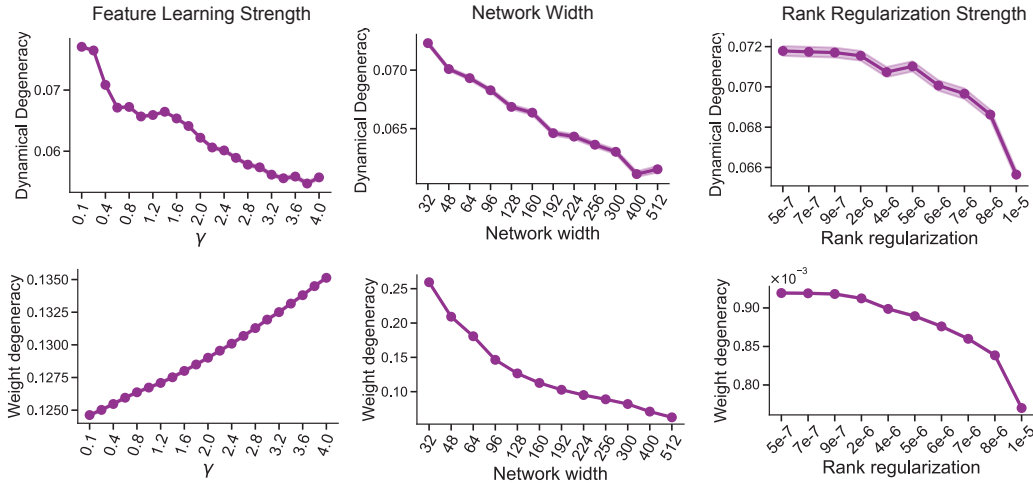


Figure 14: Feature learning, network width, and regularization strength’s effect on degeneracy over a denser sweep of conditions on the 3-Bits Flip Flop task.

## J Detailed characterization of OOD generalization performance

In addition to showing the behavioral degeneracy in the main text, here we provide a more detailed characterization of the OOD behavior of networks by showing the mean versus standard deviation, and the distribution of the OOD losses.

### J.1 Changing task complexity

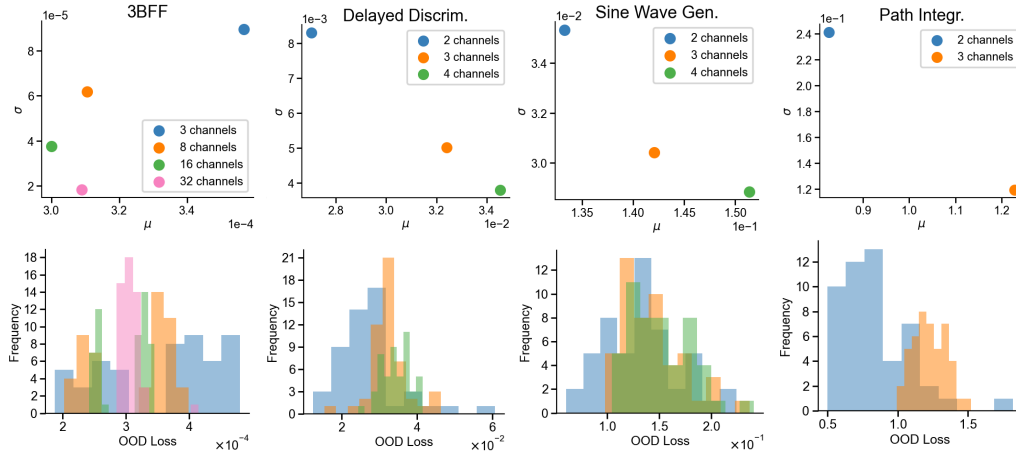


Figure 15: Detailed characterization of the OOD performance of networks while changing task complexity.

### J.2 Changing feature learning strength

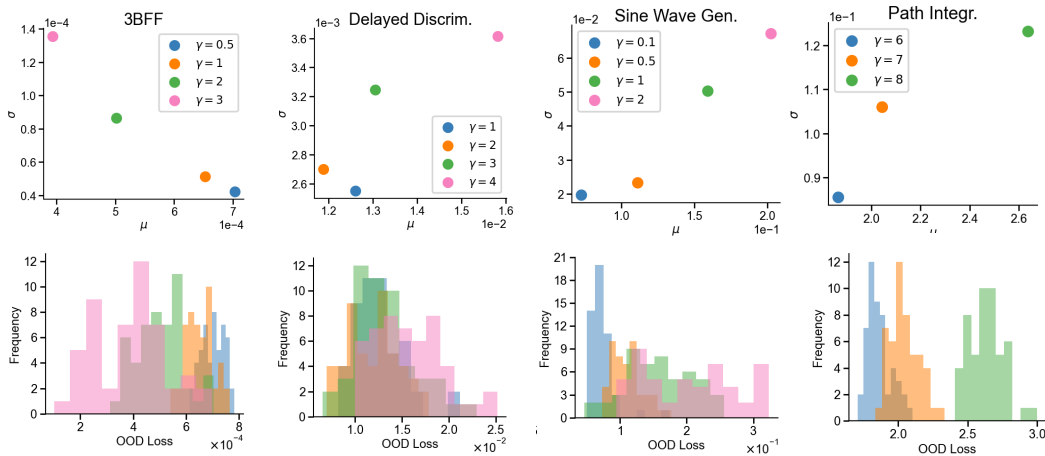


Figure 16: Detailed characterization of the OOD performance of networks while changing feature learning strength. Across Delayed Discrimination, Sine Wave Generation, and Path Integration tasks, networks trained with larger  $\gamma$  – and thus undergoing stronger feature learning – exhibit higher mean OOD generalization loss together with higher variability, potentially reflecting overfitting to the training task.

### J.3 Changing network size

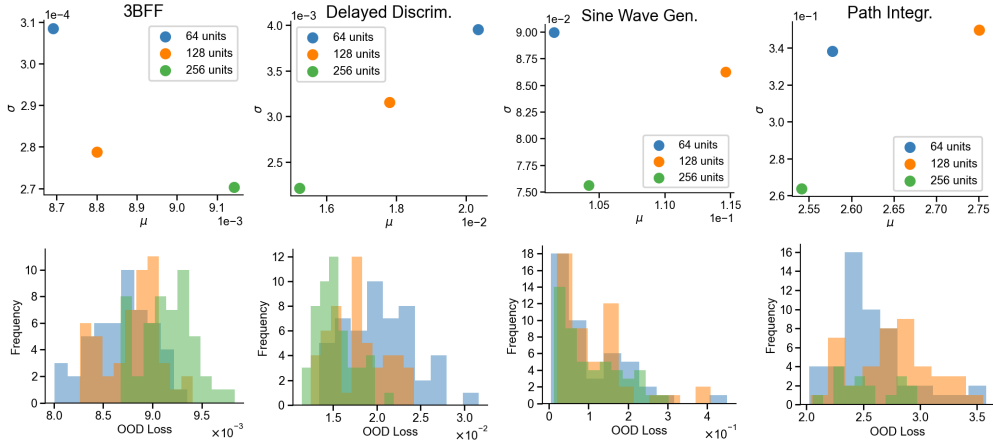


Figure 17: Detailed characterization of the OOD performance of networks while changing network size.

### J.4 Changing regularization strength

#### J.4.1 Low-rank regularization

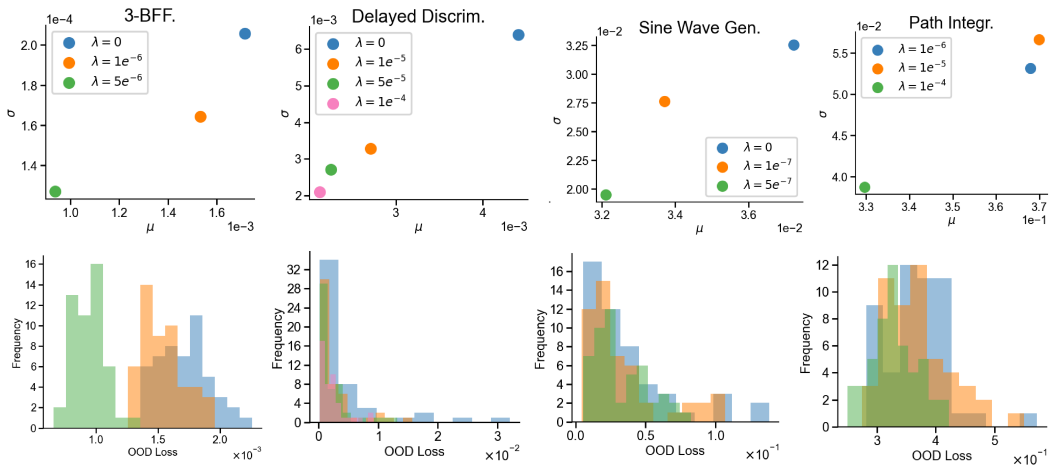


Figure 18: Detailed characterization of the OOD performance of networks while changing low-rank regularization strength.

## J.4.2 Sparsity (L1) regularization

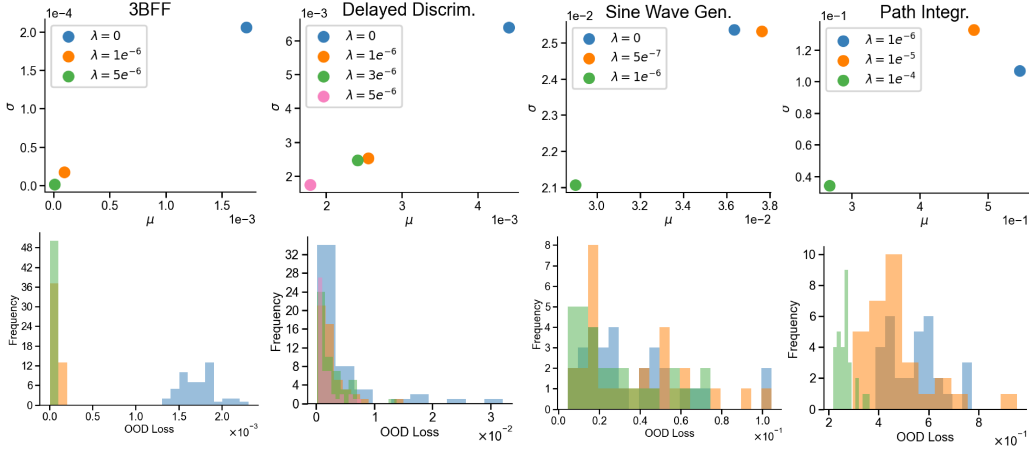


Figure 19: Detailed characterization of the OOD performance of networks while changing sparsity (L1) regularization strength.

## K A short introduction to Maximal Update Parameterization ( $\mu P$ )

Under the NTK parametrization, as the network width goes to infinity, the network operates in the *lazy* regime, where its functional evolution is well-approximated by a first-order Taylor expansion around the initial parameters [73, 59, 54, 55]. In this limit feature learning is suppressed and training dynamics are governed by the fixed Neural Tangent Kernel (NTK).

To preserve non-trivial feature learning at large width, the *Maximal Update Parameterization* ( $\mu P$ ) rescales both the weight initialization and the learning rate.  $\mu P$  keeps three quantities *width-invariant* at every layer—(i) the norm/variance of activations (ii) the norm/variance of the gradients, and (iii) the parameter updates applied by the optimizer [100, 101, 56, 57].

For recurrent neural networks, under Stochastic Gradient Descent (SGD), the network output, initialization, and learning rates are scaled as

$$f = \frac{1}{\gamma_0 N} \vec{w} \cdot \phi(h), \quad (1)$$

$$\partial_t h = -h + \frac{1}{\sqrt{N}} J \phi(h), \quad J_{ij} \sim \mathcal{N}(0, 1), \quad (2)$$

$$\eta_{\text{SGD}} = \eta_0 \gamma_0^2 N. \quad (3)$$

Under Adam optimizer, the network output, initialization, and learning rates are scaled as

$$f = \frac{1}{\gamma_0 N} \vec{w} \cdot \phi(h), \quad (4)$$

$$\partial_t h = -h + \frac{1}{N} J \phi(h), \quad J_{ij} \sim \mathcal{N}(0, N), \quad (5)$$

$$\eta_{\text{Adam}} = \eta_0 \gamma_0. \quad (6)$$

## L Theoretical relationship between parameterizations

We compare two RNN formalisms used in different parts of the main manuscript: a standard discrete-time RNN trained with fixed learning rate and conventional initialization, and a  $\mu P$ -style RNN trained with leaky integrator dynamics and width-aware scaling.

In the standard discrete-time RNN, the hidden activations are updated as

$$h(t+1) = \phi(W_h h(t) + W_x x(t)),$$

In  $\mu P$  RNNs, the hidden activations are updated as

$$h(t+1) - h(t) = \tau(-h(t) + \frac{1}{N}J\phi(h(t)) + Ux(t))$$

When  $\tau = 1$ ,

$$\begin{aligned} h(t+1) - h(t) &= -h(t) + \frac{1}{N}J\phi(h(t)) + Ux(t) \\ h(t+1) &= \frac{1}{N}J\phi(h(t)) + Ux(t) \end{aligned}$$

Aside from the overall scaling factor, the difference between the two parameterizations lies in the placement of the non-linearity:

- **Standard RNN:**  $\phi$  is applied *post-activation*, i.e. after the recurrent and input terms are linearly combined,
- **$\mu P$  RNN:**  $\phi$  is applied *pre-activation*; i.e. before the recurrent weight matrix, so the hidden state is first non-linearized and then linearly combined

Miller and Fumarola [102] demonstrated that two classes of continuous-time firing-rate models which differ in their placement of the non-linearity are mathematically equivalent under a change of variables:

$$\text{v-model} \quad \tau \frac{dv}{dt} = -v + \tilde{I}(t) + Wf(v)$$

$$\text{r-model:} \quad \tau \frac{dr}{dt} = -r + f(Wr + I(t))$$

with equivalence holding under the transformation  $v(t) = Wr(t) + I(t)$  and  $\tilde{I}(t) = I(t) + \tau \frac{dI}{dt}$ , assuming matched initial conditions.

Briefly, they show that  $Wr + I$  evolves according to the  $v$ -equation as follows:

$$\begin{aligned} v(t) &= Wr(t) + I(t) \\ \frac{dv}{dt} &= \frac{d}{dt}(Wr(t) + I(t)) \\ &= W \frac{dr}{dt} + \frac{dI}{dt} \\ &= W \left( \frac{1}{\tau} (-r + f(Wr + I)) \right) + \frac{dI}{dt} \\ \tau \frac{dv}{dt} &= -Wr + Wf(Wr + I) + \tau \frac{dI}{dt} \\ &= -(v - I) + Wf(v) + \tau \frac{dI}{dt} \\ &= -v + I + \tau \frac{dI}{dt} + Wf(v) \\ \tau \frac{dv}{dt} &= -v + \tilde{I}(t) + Wf(v) \end{aligned}$$

This mapping applies directly to RNNs viewed as continuous-time dynamical systems and helps relate v-type  $\mu P$ -style RNNs to standard discrete-time RNNs. It suggests that the  $\mu P$  RNN (in v-type form) and the standard RNN (in r-type form) can be treated as different parameterizations of the same underlying dynamical system when:

- Initialization scales are matched
- The learning rate is scaled appropriately with  $\gamma$

- Output weight norms are adjusted according to width

In summary, while a theoretical equivalence exists, it is contingent on consistent scaling across all components of the model. In this manuscript, we use the standard discrete-time RNNs due to its practical relevance for task-driven modeling community, while switching to  $\mu P$  to isolate the effect of feature learning and network size. Additionally, we confirm that the feature learning and network size effects on degeneracy hold qualitatively the same in standard discrete-time RNNs, unless where altering network width induces unstable and lazier learning in larger networks (Figure P and Q).

## M Verifying larger $\gamma$ reliably induces stronger feature learning in $\mu P$

In  $\mu P$  parameterization, the parameter  $\gamma$  interpolates between lazy training and rich, feature-learning dynamics, without itself being the absolute magnitude of feature learning. Here, we assess feature-learning strength in RNNs under varying  $\gamma$  using two complementary metrics:

**Weight-change norm** which measures the magnitude of weight change throughout training. A larger weight change norm indicates that the network undergoes richer learning or more feature learning.

$$\frac{\|\mathbf{W}_T - \mathbf{W}_0\|_F}{N},$$

where  $N$  is the number of parameters in the weight matrices being compared.

**Kernel alignment (KA)**, which measures the directional change of the neural tangent kernel (NTK) before and after training. A lower KA score corresponds to a larger NTK rotation and thus stronger feature learning.

$$\text{KA}(K^{(f)}, K^{(0)}) = \frac{\text{Tr}(K^{(f)} K^{(0)})}{\|K^{(f)}\|_F \|K^{(0)}\|_F}, \quad K = \nabla_W \hat{y}^\top \nabla_W \hat{y}.$$

We demonstrate that higher  $\gamma$  indeed amplifies feature learning inside the network.

### M.1 N-BFF

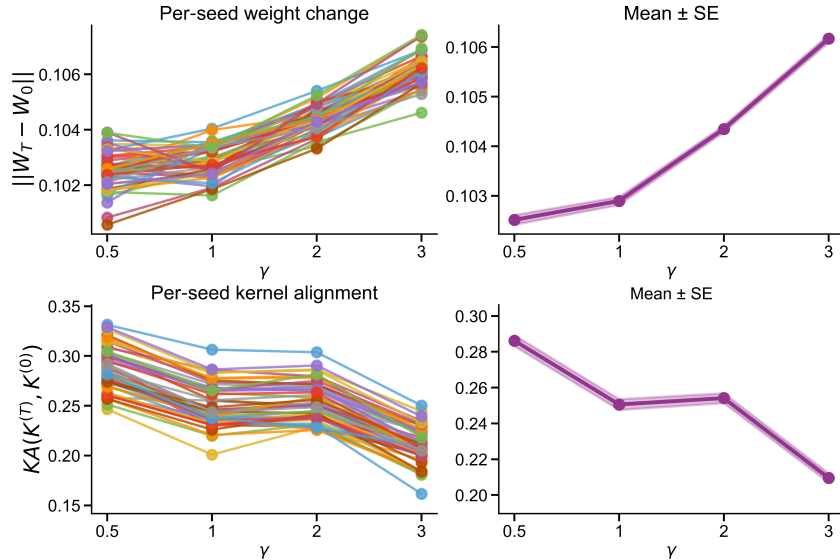


Figure 20: Weight change norm and kernel alignment for networks trained on the 3-Bits Flip Flop task as we vary  $\gamma$ . On the left panels, we show the per-seed metrics where connected dots of the same color are networks of identical initialization trained with different  $\gamma$ . On the right panels, we show the mean and standard error of the metrics across 50 networks. For larger  $\gamma$ , the weights move further from their initializations as shown by the larger weight change norm, and their NTK evolves more distinct from the network’s NTK at initialization as shown by the reduced KA. Both indicate stronger feature learning for networks trained under larger  $\gamma$ .

## M.2 Delayed Discrimination

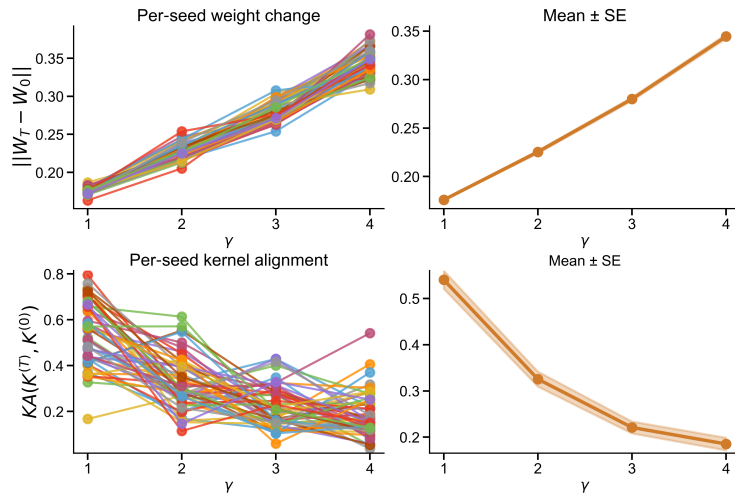


Figure 21: Stronger feature learning for networks trained under larger  $\gamma$  on the Delayed Discrimination task.

## M.3 Sine Wave Generation

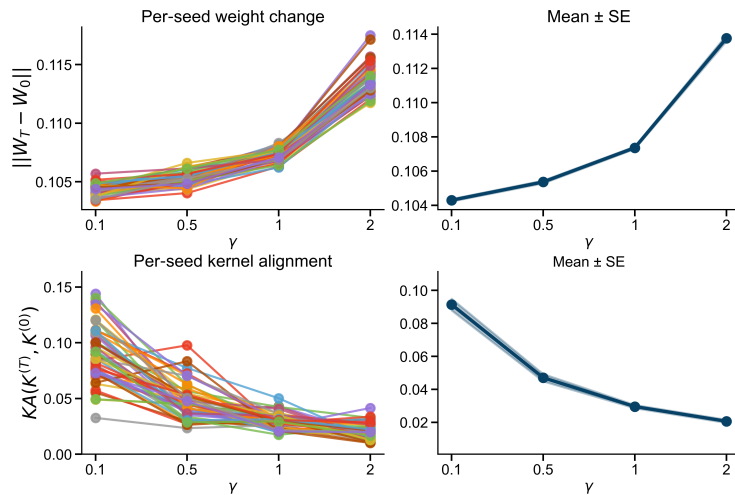


Figure 22: Stronger feature learning for networks trained under larger  $\gamma$  on the Sine Wave Generation task.

## M.4 Path Integration

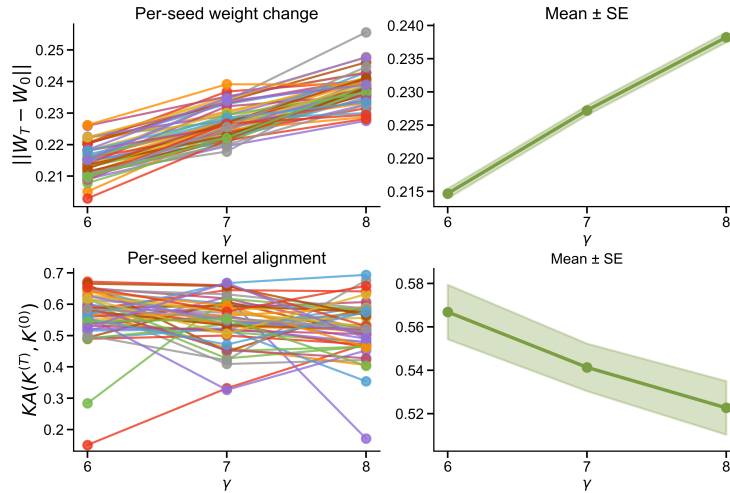


Figure 23: Stronger feature learning for networks trained under larger  $\gamma$  on the Path Integration task.

## N Verifying $\mu P$ reliably controls for feature learning across network width

Here, we only use Kernel Alignment to assess the feature learning strength in the networks since the unnormalized weight-change norm  $\|\mathbf{W}_T - \mathbf{W}_0\|_F$  scales directly with matrix size (therefore network size) and there exists no obvious way to normalize across different dimensions. In our earlier analysis where we compared weight-change norms at varying  $\gamma$ , network size remained fixed, so those Frobenius-norm measures were directly comparable. We found that, for all tasks except Delayed Discrimination, the change in mean KA across different network sizes remains extremely small (less than 0.1), which demonstrates that  $\mu P$  parameterization with the same  $\gamma$  has effectively controlled for feature learning strength across network sizes. On Delayed Discrimination, the networks undergo slightly lazier learning for larger network sizes. Nevertheless, we still include Delayed Discrimination in our analyses of solution degeneracy to ensure *our conclusions remain robust even when  $\mu P$  can't perfectly equalize feature-learning strength across widths*. As shown in the main paper, lazier learning regime generally increases dynamical degeneracy; yet, larger networks which exhibit lazier learning in the N-BFF task actually display lower dynamical degeneracy. This reversed trend confirms that the changes in solution degeneracy arise from network size itself, not from residual variation in feature learning strength.

### N.1 N-BFF

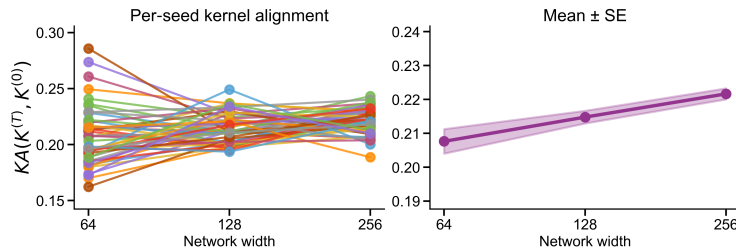


Figure 24: Kernel alignment (KA) for different network width on the 3 Bits Flip-Flop task. (Lower KA implies more feature learning.)

## N.2 Delayed Discrimination

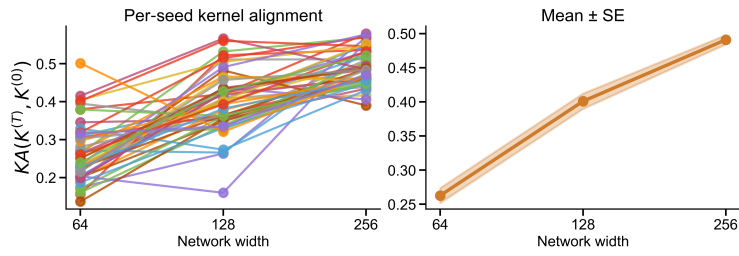


Figure 25: Kernel alignment for different network width on the Delayed Discrimination task.

## N.3 Sine Wave Generation

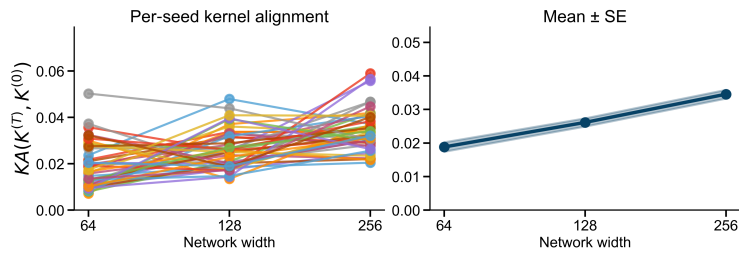


Figure 26: Kernel alignment for different network width on the Sine Wave Generation task.

## N.4 Path Integration

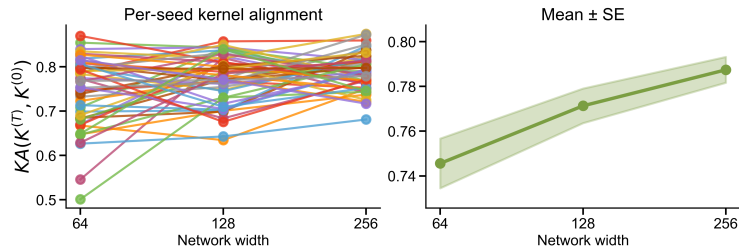


Figure 27: Kernel alignment for different network width on the Path Integration task.

## O Regularization's effect on degeneracy for all tasks

In addition to showing regularization's effect on degeneracy in Delayed Discrimination task in the main paper, here we show that heavier low-rank regularization and sparsity regularization also reliably reduce solution degeneracy across neural dynamics, weights, and OOD behavior in the other three tasks.

### O.1 Low-rank regularization

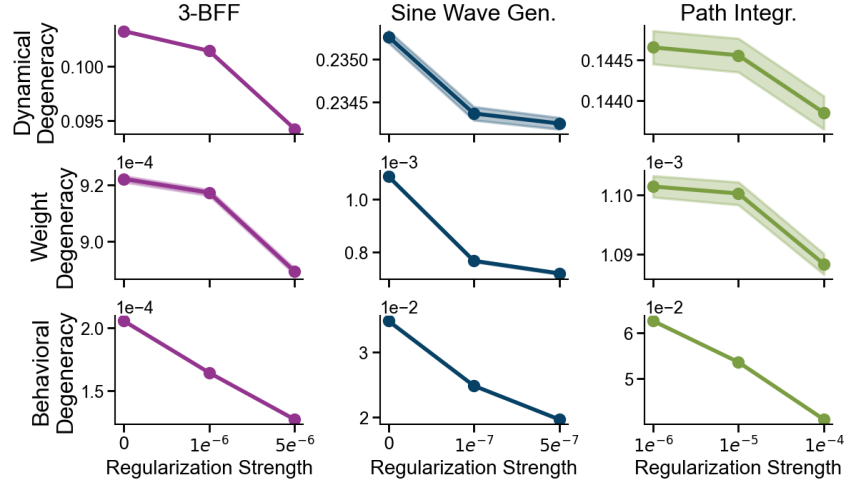


Figure 28: Low-rank regularization reduces degeneracy across neural dynamics, weight, and OOD behavior on the N-BFF, Sinewave Generation, and Path Integration task.

### O.2 Sparsity regularization

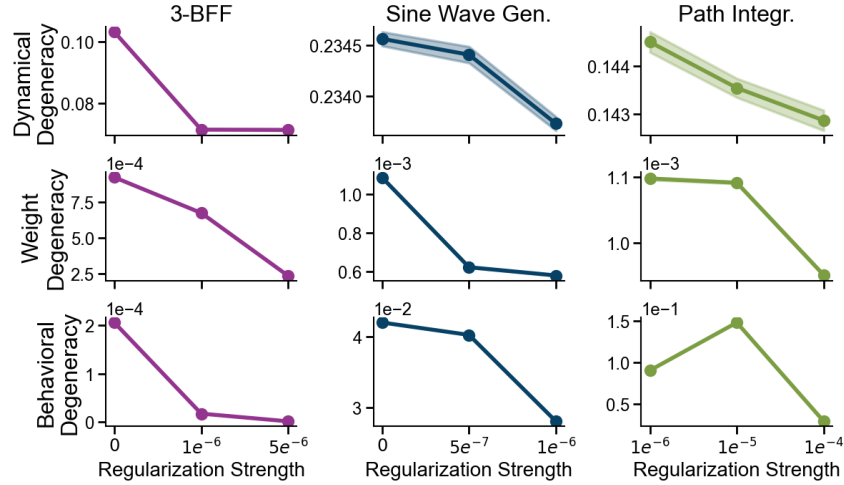


Figure 29: Sparsity regularization reduces degeneracy across neural dynamics, weight, and OOD behavior on the N-BFF, Sinewave Generation, and Path Integration task.

## P Test feature learning effect on degeneracy in standard parameterization

While  $\mu P$  lets us systematically vary feature-learning strength to study its impact on solution degeneracy, we confirm that the same qualitative pattern appears in *standard* discrete-time RNNs: stronger feature learning **lowers dynamical degeneracy** and **raises weight degeneracy** (Figure 30).

To manipulate feature-learning strength in these ordinary RNNs we applied the  $\gamma$ -**trick**—scaling the network’s outputs by  $\gamma$ —and multiplied the learning rate by the same factor. With width fixed, these two operations replicate the effective changes induced by  $\mu P$ . Figure 31 shows that this combination reliably tunes feature-learning strength. Besides weight-change norm and kernel alignment, we also report **representation alignment (RA)**, giving a more fine-grained view of how much the learned features deviate from their initialization [62]. Representation alignment is the directional change of the network’s representational dissimilarity matrix before and after training, and is defined by

$$\text{RA}(R^{(T)}, R^{(0)}) := \frac{\text{Tr}(R^{(T)} R^{(0)})}{\|R^{(T)}\| \|R^{(0)}\|}, \quad R := H^\top H,$$

A lower RA means more change in the network’s representation of inputs before and after training, and indicates stronger feature learning.

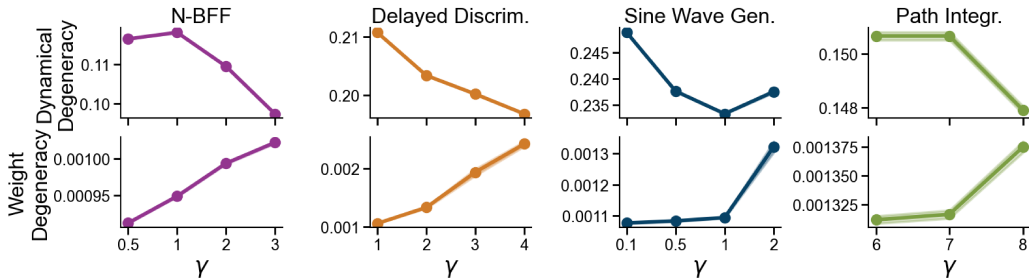


Figure 30: Stronger feature learning reliably decreases dynamical degeneracy while increasing weight degeneracy in standard discrete-time RNNs.

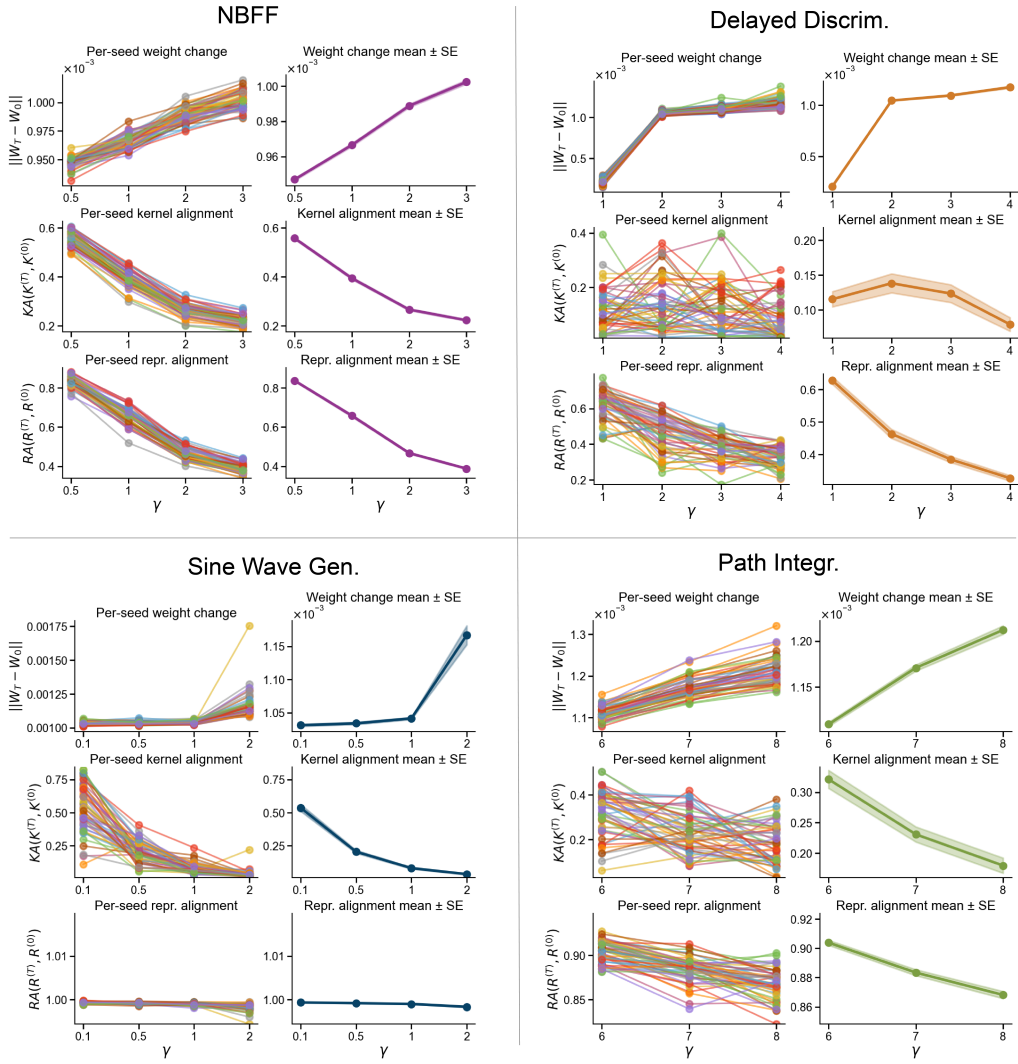


Figure 31: Larger  $\gamma$  reliably induces stronger feature learning in standard discrete-time RNNs.

## Q Test network size effect on degeneracy in standard parameterization

When we vary network width, both the standard parameterization and  $\mu P$  parameterization display the same overall pattern: **larger networks exhibit lower dynamical and weight degeneracy**. An exception arises in the 3BFF task, where feature learning becomes unstable and collapses in the wider models. In that setting we instead see *higher* dynamical degeneracy, which we suspect because the feature learning effect (lazier learning leads to higher dynamical degeneracy) dominates the network size effect.

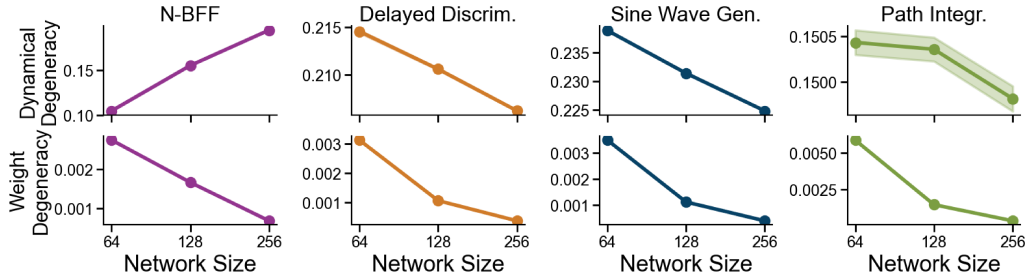


Figure 32: Larger network sizes lead to lower dynamical and weight degeneracy, except in the case where feature learning is unstable across width (in N-BFF).

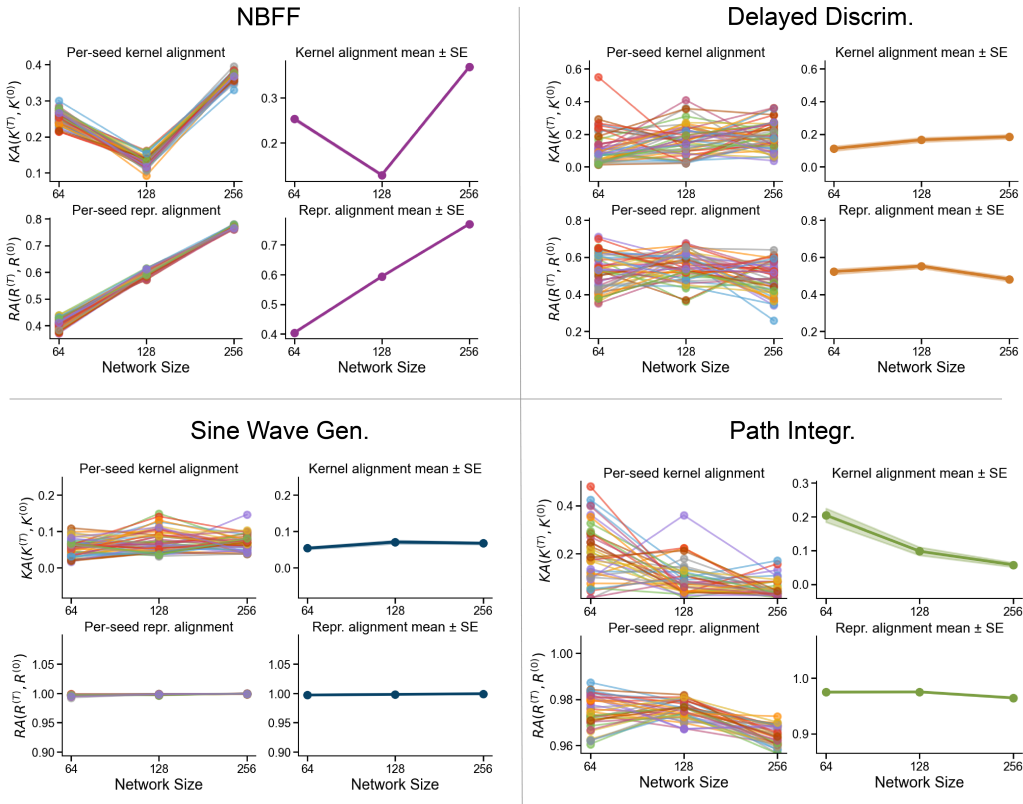


Figure 33: When changing network width in standard discrete-time RNNs, feature learning strength remains stable across width except in N-BFF, where notably lazier learning happens in the widest network.

## **R Disclosure of compute resources**

In this study, we conducted 50 independent training runs on each of four tasks, systematically sweeping four factors that modulate solution degeneracy—task complexity (15 experiments), learning regime (15 experiments), network size (12 experiments), and regularization strength (26 experiments), resulting in a total of 3400 networks. Each experiment was allocated 5 NVIDIA V100/A100 GPUs, 32 CPU cores, 256 GB of RAM, and a 4-hour wall-clock limit, for a total compute cost of approximately 68 000 GPU-hours.

## NeurIPS Paper Checklist

### 1. Claims

Question: Do the main claims made in the abstract and introduction accurately reflect the paper's contributions and scope?

Answer: [Yes]

Justification: The main claims made in the abstract and introduction are accurate descriptions on the data and result presented in the rest of the paper.

Guidelines:

- The answer NA means that the abstract and introduction do not include the claims made in the paper.
- The abstract and/or introduction should clearly state the claims made, including the contributions made in the paper and important assumptions and limitations. A No or NA answer to this question will not be perceived well by the reviewers.
- The claims made should match theoretical and experimental results, and reflect how much the results can be expected to generalize to other settings.
- It is fine to include aspirational goals as motivation as long as it is clear that these goals are not attained by the paper.

### 2. Limitations

Question: Does the paper discuss the limitations of the work performed by the authors?

Answer: [Yes]

Justification: We have discussed the limitations and further directions of the paper in the Discussion section.

Guidelines:

- The answer NA means that the paper has no limitation while the answer No means that the paper has limitations, but those are not discussed in the paper.
- The authors are encouraged to create a separate "Limitations" section in their paper.
- The paper should point out any strong assumptions and how robust the results are to violations of these assumptions (e.g., independence assumptions, noiseless settings, model well-specification, asymptotic approximations only holding locally). The authors should reflect on how these assumptions might be violated in practice and what the implications would be.
- The authors should reflect on the scope of the claims made, e.g., if the approach was only tested on a few datasets or with a few runs. In general, empirical results often depend on implicit assumptions, which should be articulated.
- The authors should reflect on the factors that influence the performance of the approach. For example, a facial recognition algorithm may perform poorly when image resolution is low or images are taken in low lighting. Or a speech-to-text system might not be used reliably to provide closed captions for online lectures because it fails to handle technical jargon.
- The authors should discuss the computational efficiency of the proposed algorithms and how they scale with dataset size.
- If applicable, the authors should discuss possible limitations of their approach to address problems of privacy and fairness.
- While the authors might fear that complete honesty about limitations might be used by reviewers as grounds for rejection, a worse outcome might be that reviewers discover limitations that aren't acknowledged in the paper. The authors should use their best judgment and recognize that individual actions in favor of transparency play an important role in developing norms that preserve the integrity of the community. Reviewers will be specifically instructed to not penalize honesty concerning limitations.

### 3. Theory assumptions and proofs

Question: For each theoretical result, does the paper provide the full set of assumptions and a complete (and correct) proof?

Answer: [NA]

Justification: We will be exploring an theoretical validation of the result that strong feature learning induces lower dynamical degeneracy and higher weight degeneracy in linear RNNs in a follow-up paper.

Guidelines:

- The answer NA means that the paper does not include theoretical results.
- All the theorems, formulas, and proofs in the paper should be numbered and cross-referenced.
- All assumptions should be clearly stated or referenced in the statement of any theorems.
- The proofs can either appear in the main paper or the supplemental material, but if they appear in the supplemental material, the authors are encouraged to provide a short proof sketch to provide intuition.
- Inversely, any informal proof provided in the core of the paper should be complemented by formal proofs provided in appendix or supplemental material.
- Theorems and Lemmas that the proof relies upon should be properly referenced.

#### 4. Experimental result reproducibility

Question: Does the paper fully disclose all the information needed to reproduce the main experimental results of the paper to the extent that it affects the main claims and/or conclusions of the paper (regardless of whether the code and data are provided or not)?

Answer: [Yes]

Justification: Yes, we have described the network equation, task details, training procedures, and all hyperparameter choices both in the main text and in the Appendix.

Guidelines:

- The answer NA means that the paper does not include experiments.
- If the paper includes experiments, a No answer to this question will not be perceived well by the reviewers: Making the paper reproducible is important, regardless of whether the code and data are provided or not.
- If the contribution is a dataset and/or model, the authors should describe the steps taken to make their results reproducible or verifiable.
- Depending on the contribution, reproducibility can be accomplished in various ways. For example, if the contribution is a novel architecture, describing the architecture fully might suffice, or if the contribution is a specific model and empirical evaluation, it may be necessary to either make it possible for others to replicate the model with the same dataset, or provide access to the model. In general, releasing code and data is often one good way to accomplish this, but reproducibility can also be provided via detailed instructions for how to replicate the results, access to a hosted model (e.g., in the case of a large language model), releasing of a model checkpoint, or other means that are appropriate to the research performed.
- While NeurIPS does not require releasing code, the conference does require all submissions to provide some reasonable avenue for reproducibility, which may depend on the nature of the contribution. For example
  - (a) If the contribution is primarily a new algorithm, the paper should make it clear how to reproduce that algorithm.
  - (b) If the contribution is primarily a new model architecture, the paper should describe the architecture clearly and fully.
  - (c) If the contribution is a new model (e.g., a large language model), then there should either be a way to access this model for reproducing the results or a way to reproduce the model (e.g., with an open-source dataset or instructions for how to construct the dataset).
  - (d) We recognize that reproducibility may be tricky in some cases, in which case authors are welcome to describe the particular way they provide for reproducibility. In the case of closed-source models, it may be that access to the model is limited in some way (e.g., to registered users), but it should be possible for other researchers to have some path to reproducing or verifying the results.

## 5. Open access to data and code

Question: Does the paper provide open access to the data and code, with sufficient instructions to faithfully reproduce the main experimental results, as described in supplemental material?

Answer: [Yes]

Justification: The code is attached as part of the supplemental materials.

Guidelines:

- The answer NA means that paper does not include experiments requiring code.
- Please see the NeurIPS code and data submission guidelines (<https://nips.cc/public/guides/CodeSubmissionPolicy>) for more details.
- While we encourage the release of code and data, we understand that this might not be possible, so “No” is an acceptable answer. Papers cannot be rejected simply for not including code, unless this is central to the contribution (e.g., for a new open-source benchmark).
- The instructions should contain the exact command and environment needed to run to reproduce the results. See the NeurIPS code and data submission guidelines (<https://nips.cc/public/guides/CodeSubmissionPolicy>) for more details.
- The authors should provide instructions on data access and preparation, including how to access the raw data, preprocessed data, intermediate data, and generated data, etc.
- The authors should provide scripts to reproduce all experimental results for the new proposed method and baselines. If only a subset of experiments are reproducible, they should state which ones are omitted from the script and why.
- At submission time, to preserve anonymity, the authors should release anonymized versions (if applicable).
- Providing as much information as possible in supplemental material (appended to the paper) is recommended, but including URLs to data and code is permitted.

## 6. Experimental setting/details

Question: Does the paper specify all the training and test details (e.g., data splits, hyperparameters, how they were chosen, type of optimizer, etc.) necessary to understand the results?

Answer: [Yes]

Justification: Yes, we have provided training and test details, the optimizers, and all the choices of the hyperparameters in the Method section of the paper and in the Appendix.

Guidelines:

- The answer NA means that the paper does not include experiments.
- The experimental setting should be presented in the core of the paper to a level of detail that is necessary to appreciate the results and make sense of them.
- The full details can be provided either with the code, in appendix, or as supplemental material.

## 7. Experiment statistical significance

Question: Does the paper report error bars suitably and correctly defined or other appropriate information about the statistical significance of the experiments?

Answer: [Yes]

Justification: We have included standard error in all figures where the goal is to demonstrate that a given quantity—whether degeneracy, weight change norm, or kernel alignment—differs significantly across varying levels of task complexity, feature learning strength, network size, and regularization.

Guidelines:

- The answer NA means that the paper does not include experiments.
- The authors should answer "Yes" if the results are accompanied by error bars, confidence intervals, or statistical significance tests, at least for the experiments that support the main claims of the paper.

- The factors of variability that the error bars are capturing should be clearly stated (for example, train/test split, initialization, random drawing of some parameter, or overall run with given experimental conditions).
- The method for calculating the error bars should be explained (closed form formula, call to a library function, bootstrap, etc.)
- The assumptions made should be given (e.g., Normally distributed errors).
- It should be clear whether the error bar is the standard deviation or the standard error of the mean.
- It is OK to report 1-sigma error bars, but one should state it. The authors should preferably report a 2-sigma error bar than state that they have a 96% CI, if the hypothesis of Normality of errors is not verified.
- For asymmetric distributions, the authors should be careful not to show in tables or figures symmetric error bars that would yield results that are out of range (e.g. negative error rates).
- If error bars are reported in tables or plots, The authors should explain in the text how they were calculated and reference the corresponding figures or tables in the text.

#### 8. Experiments compute resources

Question: For each experiment, does the paper provide sufficient information on the computer resources (type of compute workers, memory, time of execution) needed to reproduce the experiments?

Answer: [Yes]

Justification: Yes, we have described the experiments compute resources in the Appendix.

Guidelines:

- The answer NA means that the paper does not include experiments.
- The paper should indicate the type of compute workers CPU or GPU, internal cluster, or cloud provider, including relevant memory and storage.
- The paper should provide the amount of compute required for each of the individual experimental runs as well as estimate the total compute.
- The paper should disclose whether the full research project required more compute than the experiments reported in the paper (e.g., preliminary or failed experiments that didn't make it into the paper).

#### 9. Code of ethics

Question: Does the research conducted in the paper conform, in every respect, with the NeurIPS Code of Ethics <https://neurips.cc/public/EthicsGuidelines>?

Answer: [Yes]

Justification: The research conducted in the paper conform, in every respect, with the NeurIPS Code of Ethics.

Guidelines:

- The answer NA means that the authors have not reviewed the NeurIPS Code of Ethics.
- If the authors answer No, they should explain the special circumstances that require a deviation from the Code of Ethics.
- The authors should make sure to preserve anonymity (e.g., if there is a special consideration due to laws or regulations in their jurisdiction).

#### 10. Broader impacts

Question: Does the paper discuss both potential positive societal impacts and negative societal impacts of the work performed?

Answer: [NA]

Justification: The paper focuses on scientific and methodological contributions—namely, a framework for measuring and controlling solution degeneracy in RNNs and its implications for computational neuroscience. As such models are typically used as a hypothesis generation tool for the potential neural mechanisms underlying certain computations, we do not foresee immediate applications that would raise negative social impacts.

Guidelines:

- The answer NA means that there is no societal impact of the work performed.
- If the authors answer NA or No, they should explain why their work has no societal impact or why the paper does not address societal impact.
- Examples of negative societal impacts include potential malicious or unintended uses (e.g., disinformation, generating fake profiles, surveillance), fairness considerations (e.g., deployment of technologies that could make decisions that unfairly impact specific groups), privacy considerations, and security considerations.
- The conference expects that many papers will be foundational research and not tied to particular applications, let alone deployments. However, if there is a direct path to any negative applications, the authors should point it out. For example, it is legitimate to point out that an improvement in the quality of generative models could be used to generate deepfakes for disinformation. On the other hand, it is not needed to point out that a generic algorithm for optimizing neural networks could enable people to train models that generate Deepfakes faster.
- The authors should consider possible harms that could arise when the technology is being used as intended and functioning correctly, harms that could arise when the technology is being used as intended but gives incorrect results, and harms following from (intentional or unintentional) misuse of the technology.
- If there are negative societal impacts, the authors could also discuss possible mitigation strategies (e.g., gated release of models, providing defenses in addition to attacks, mechanisms for monitoring misuse, mechanisms to monitor how a system learns from feedback over time, improving the efficiency and accessibility of ML).

## 11. Safeguards

Question: Does the paper describe safeguards that have been put in place for responsible release of data or models that have a high risk for misuse (e.g., pretrained language models, image generators, or scraped datasets)?

Answer: [NA]

Justification: In this paper, we study the solution landscape of RNNs trained on neuroscience-inspired tasks, which lacks such risk for misuse.

Guidelines:

- The answer NA means that the paper poses no such risks.
- Released models that have a high risk for misuse or dual-use should be released with necessary safeguards to allow for controlled use of the model, for example by requiring that users adhere to usage guidelines or restrictions to access the model or implementing safety filters.
- Datasets that have been scraped from the Internet could pose safety risks. The authors should describe how they avoided releasing unsafe images.
- We recognize that providing effective safeguards is challenging, and many papers do not require this, but we encourage authors to take this into account and make a best faith effort.

## 12. Licenses for existing assets

Question: Are the creators or original owners of assets (e.g., code, data, models), used in the paper, properly credited and are the license and terms of use explicitly mentioned and properly respected?

Answer: [Yes]

Justification: Our task implementation and the metrics we use to compare independently trained RNNs involve reuse of code published with previous paper. We have properly cited the paper that produced the code package.

Guidelines:

- The answer NA means that the paper does not use existing assets.
- The authors should cite the original paper that produced the code package or dataset.

- The authors should state which version of the asset is used and, if possible, include a URL.
- The name of the license (e.g., CC-BY 4.0) should be included for each asset.
- For scraped data from a particular source (e.g., website), the copyright and terms of service of that source should be provided.
- If assets are released, the license, copyright information, and terms of use in the package should be provided. For popular datasets, [paperswithcode.com/datasets](https://paperswithcode.com/datasets) has curated licenses for some datasets. Their licensing guide can help determine the license of a dataset.
- For existing datasets that are re-packaged, both the original license and the license of the derived asset (if it has changed) should be provided.
- If this information is not available online, the authors are encouraged to reach out to the asset's creators.

### 13. **New assets**

Question: Are new assets introduced in the paper well documented and is the documentation provided alongside the assets?

Answer: [Yes]

Justification: We have attached our code as part of the supplemental materials and have provided documentations on how to run it.

Guidelines:

- The answer NA means that the paper does not release new assets.
- Researchers should communicate the details of the dataset/code/model as part of their submissions via structured templates. This includes details about training, license, limitations, etc.
- The paper should discuss whether and how consent was obtained from people whose asset is used.
- At submission time, remember to anonymize your assets (if applicable). You can either create an anonymized URL or include an anonymized zip file.

### 14. **Crowdsourcing and research with human subjects**

Question: For crowdsourcing experiments and research with human subjects, does the paper include the full text of instructions given to participants and screenshots, if applicable, as well as details about compensation (if any)?

Answer: [NA]

Justification: The paper does not involve crowdsourcing nor research with human subjects.

Guidelines:

- The answer NA means that the paper does not involve crowdsourcing nor research with human subjects.
- Including this information in the supplemental material is fine, but if the main contribution of the paper involves human subjects, then as much detail as possible should be included in the main paper.
- According to the NeurIPS Code of Ethics, workers involved in data collection, curation, or other labor should be paid at least the minimum wage in the country of the data collector.

### 15. **Institutional review board (IRB) approvals or equivalent for research with human subjects**

Question: Does the paper describe potential risks incurred by study participants, whether such risks were disclosed to the subjects, and whether Institutional Review Board (IRB) approvals (or an equivalent approval/review based on the requirements of your country or institution) were obtained?

Answer: [NA]

Justification: The paper does not involve crowdsourcing nor research with human subjects.

Guidelines:

- The answer NA means that the paper does not involve crowdsourcing nor research with human subjects.
- Depending on the country in which research is conducted, IRB approval (or equivalent) may be required for any human subjects research. If you obtained IRB approval, you should clearly state this in the paper.
- We recognize that the procedures for this may vary significantly between institutions and locations, and we expect authors to adhere to the NeurIPS Code of Ethics and the guidelines for their institution.
- For initial submissions, do not include any information that would break anonymity (if applicable), such as the institution conducting the review.

#### 16. **Declaration of LLM usage**

Question: Does the paper describe the usage of LLMs if it is an important, original, or non-standard component of the core methods in this research? Note that if the LLM is used only for writing, editing, or formatting purposes and does not impact the core methodology, scientific rigorousness, or originality of the research, declaration is not required.

Answer: [NA]

Justification: The core method development in this research does not involve LLMs as any important, original, or non-standard components.

Guidelines:

- The answer NA means that the core method development in this research does not involve LLMs as any important, original, or non-standard components.
- Please refer to our LLM policy (<https://neurips.cc/Conferences/2025/LLM>) for what should or should not be described.